Journal of The Electrochemical Society

The Electrochemical Society
Advancing solid state & electrochemical science & technology

Review—Origin and Promotional Effects of Plasmonics in Photocatalysis

To cite this article before publication: Madasamy Thangamuthu *et al* 2022 *J. Electrochem. Soc.* in press https://doi.org/10.1149/1945-7111/ac5c97

Review—Origin and Promotional Effects of Plasmonics in Photocatalysis

Journal:	*Journal of The Electrochemical Society*
Manuscript ID	JES-106632.R1
Manuscript Type:	Review Paper
Date Submitted by the Author:	21-Jan-2022
Complete List of Authors:	Thangamuthu, Madasamy; University College London, Chemical Engineering Tang, Junwang; University College London Thottungal Valappu, Raziman; Imperial College London Faculty of Natural Sciences Martin, Oliver; Swiss Federal Institute of Technology Lausanne , Nanophotonics and Metrology Laboratory,
Keywords:	Photoelectrochemistry, Plasmonics - Light Extraction, Semiconductors

Review—Origin and Promotional Effects of Plasmonics in Photocatalysis

Madasamy Thangamuthu,[1,a] T.V. Raziman,[1,b] Olivier J. F Martin,[1,z] and Junwang Tang[2,z]

[1]Nanophotonics and Metrology Laboratory, Swiss Federal Institute of Technology Lausanne (EPFL), 1015 Lausanne, Switzerland

[2]Department of Chemical Engineering, University College London, Torrington Place, London WC1E 7JE, UK

[a]Present address: Department of Chemical Engineering, University College London, Torrington Place, London WC1E 7JE, UK
[b]Present address: The Blackett Laboratory, Department of Physics and Department of Mathematics, Imperial College London, Imperial College London, London SW7 2AZ, UK

[z]E-mail: olivier.martin@epfl.ch; junwang.tang@ucl.ac.uk

Abstract

Plasmonic effects including near-field coupling, light scattering, guided mode through surface plasmon polaritons (SPPs), Förster resonant energy transfer (FRET), and thermoplasmonics are extensively used for harnessing inexhaustible solar energy for photovoltaics and photocatalysis. Recently, plasmonic hot carrier-driven photocatalysis has received additional attention thanks to its specific selectivity in the catalytic conversion of gas molecules and organic compounds, resulting from the direct injection of hot carriers into the lowest unoccupied molecular orbital of the adsorbate molecule. The excellent light trapping property and high efficiency of hot charge-carrier generation through electromagnetic surface plasmon decay have been identified as the dominant mechanisms that promote energy-intensive chemical reactions at room temperature and atmospheric pressure. However, understanding the electromagnetic effects of plasmonics and distinguishing them from chemical effects in photocatalysis is challenging. While there exist several reviews underlining the experimental observations of plasmonic effects, this critical review addresses the physical origin of the various plasmon-related phenomena and how they can promote photocatalysis. The conditions under which each plasmonic effect dominates and how to distinguish one from another is also discussed, together with the analysis of the photoconversion efficiency. Finally, future research directions are proposed with the aim to accelerate progress in this field at the interface between chemistry and physics.

This paper is part of the JES/JSS Joint Focus Issue In Honor of John Goodenough: A Centenarian Milestone.

1. Introduction

Free electrons inside a metal are in equilibrium and move like free gas molecules under dark conditions, and are displaced by a distance of *u* under light irradiation leading to a surface charge density $\sigma = \pm neu$ at the slab boundaries, where n is the charge density and e the electron charge (**Fig. 1a**).[1] This establishes a homogeneous electric field inside the slab. The displaced electrons experience a restoring force from the positively charged nuclei and oscillate collectively at a frequency called plasma frequency. The quanta of these charge oscillations are called *plasmons.*[2] When the plasmon modes are confined to the interface between a material with a positive value of the real part of the dielectric constant (e.g. vacuum, air, glass, or other dielectrics) and a material with a negative value (metal or heavily doped semiconductor) are termed as *surface plasmons.*[3,4] For metal nanoparticles with a regular shape and much smaller than the wavelength of the incident light, the particle–light interaction can be described using the dipole approximation.[5] The incoming electromagnetic field induces a dipole moment inside a particle, which is resonantly enhanced when the frequency of the field matches the natural frequency of surface electrons oscillating against the restoring force of positive nuclei, which is termed as *localized surface plasmon resonance (LSPR)* (**Fig. 1b**).[6] The lifetime of LSPR is tens of femtoseconds and can be computed from homogeneous linewidths measured from the scattering spectra of a plasmonic metal using a dark-field microscope.[7] Nanoparticles with non-regular shapes can support higher-order modes, beyond the dipolar mode.[8]

LSPR is damped by two processes; *radiative decay* or *scattering* into photons, dominating for larger nanoparticles in unreactive environments (*i.e.* without any molecular adsorbates on the surface), and *non-radiative decay* due to *absorption*, dominating for small particles.[9] LSPR damping can also be understood by the fact that dephasing of the polarization is caused by population decay *via* transformation of particle plasmons into photons (radiative damping) and *via* non-radiative damping into electron-hole pair generation at the surface of the nanoparticle, with their energy matching the resonant photon energy.[10,11] The decay dynamics of LSPR can be well-described by three representative time constants τ: i) the relaxation from a non-Fermi to a Fermi electron distribution through electron-electron scattering (τ < 100 fs), ii) cooling of the hot electron gas through electron-phonon scattering ($\tau \approx$ 1-10 ps), iii) heat dissipation to the environment through phonon-phonon scattering ($\tau \approx$ 100 ps).[12,13] With respect to the metal band structure, non-radiative decay has two channels as shown in **Fig. 1c** *i.e.* i) *intraband excitations*

within the conduction band and ii) *interband excitations* due to transitions between other bands and the conduction band (e.g. lower-lying d-bands to the sp conduction band for noble metal particles).[14,15] As a result, electrons are excited to unoccupied levels of the conduction band which are located above the fermi level (E_F) leaving holes at occupied levels. These electrons and holes are collectively known as plasmonic charge carriers. The plasmonic hot electron generation, distribution and relaxation mechanisms were discussed in detail using a quantum linear response theory.[16] Recent reviews highlight a wealth of opportunities for plasmonic charge carriers to induce photocatalysis directly on metal surfaces and by transferring to semiconductor surfaces.[13,17] Besides, applications of plasmonic hot-electron have also been demonstrated for sensing and photodetection.[18]

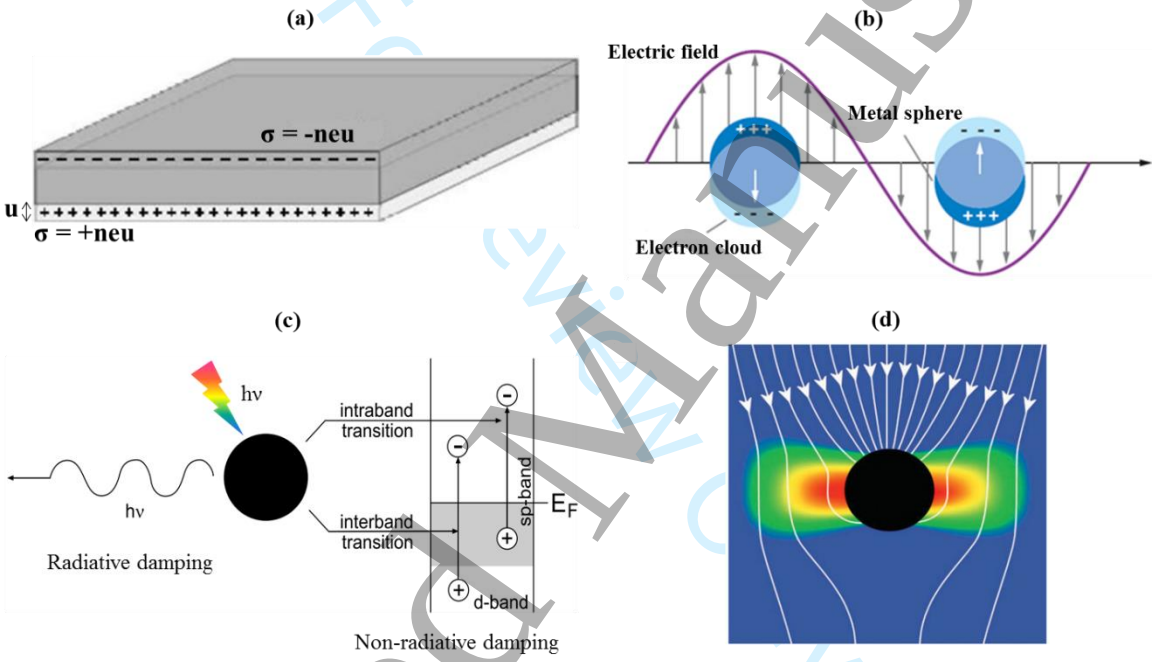

Figure 1. (a) Longitudinal collective oscillations of conduction band electrons. Adapted with permission from ref[1]. Copyright 2007 Nature Springer. (b) Illustration of localized surface plasmon of the metal nanoparticles. Adapted with permission from ref[6]. Copyright 2012 Nature Springer. (c) Schematic of radiative and non-radiative decay of localized surface plasmon of a nanoparticle. Adapted with permission from ref[15]. Copyright 2014 Elsevier. (d) Illustration of the energy flux and the electric field intensity for an incident electromagnetic wave with an electric field in the plane of the image. Adapted with permission from ref[19]. Copyright 2012 Royal Society of Chemistry.

In addition to the photocatalysis driven by plasmonic charge carriers, plasmonics can enhance the efficiency of the semiconductors in photocatalysis through near-field electromagnetic enhancement of charge carrier generation in the semiconductor.[20] In this case, plasmonic nanomaterials are used as light-trapping and electromagnetic field concentrating elements as they have extinction cross-sections greater than their geometric cross-section (**Fig. 1d**).[19,21] The electromagnetic effect and plasmonic charge carriers have been vastly used in photovoltaics

and water splitting and their mechanisms have been discussed in these reviews.[19,22–27] Furthermore, plasmonic nanomaterials have been used as nano-source of heat to induce thermal catalysis and the study of this field is termed thermo-plasmonics.[27] Recently, plasmonic hot-electron-driven photocatalysis has received additional attention as these electrons can selectively enter into the unoccupied adsorbate states and have the potential to induce chemical reactions, which are unlikely under ambient conditions. Linic and co-workers have discussed the mechanism of plasmonic hot-electron-driven photocatalytic reactions.[10,28]

Complementary to many excellent reviews which summarise the experimental results of plasmonic effect-assisted photocatalysis,[29–37] this critical review attempts to give a clear picture of the physical reason that effects involved in plasmonic nanomaterial-assisted photocatalysis. A review reported by Cushing *et al.* addresses the effects associated with plasmonics, such as light trapping (scattering), near-field coupling (plasmon-induced resonance energy transfer, PIRET), and hot electron injection for enhancing solar energy conversion efficiency of semiconductors integrated with plasmonic metal nanoparticles. It also highlights the conditions to control these plasmonic effects in detail.[38] The present review is different from that work as it more targets the understanding of the term 'hot electron' used in different scientific fields, discussing hot electron mediated photocatalysis in the absence of semiconductors and highlighting the related global debate. Furthermore, the present review also covers the plasmonic hot hole mediated oxidation reaction, thermoplasmonics, and more importantly, distinguishing the role of chemical effects from other plasmonic effects to clear the prevailing confusion. We have divided the present review into seven sections and discussed the mechanistic aspects of the plasmonic effects one by one. The photoconversion efficiency of plasmonic scattering, hot electron injection, and near-field coupling are discussed. The conditions under which each mechanism dominates are discussed and supported by reported experimental evidence from various research groups. Finally, we discuss the future of plasmonics in photocatalysis and the ways to evolve this technology for facilitating photocatalysis progress to commercial applications.

2. Electromagnetic effects for photocatalysis

Light, as a form of electromagnetic radiation, can induce chemical reactions by inducing transitions in a molecule when the photon energy matches the transition energy gap which is called photoreaction.[39] The rate of transition is proportional to the local electromagnetic field intensity ($|E|^2$) at the site of the molecule. As plasmonic nanomaterials are well known for their excellent electromagnetic field concentrating property, they can enhance the reaction by

increasing the local field.[40] Alternatively, the plasmonic particles can also enhance chemical reactions by increasing electron-hole pair generation in a nearby semiconductor which will then transfer the charge carriers to the available states in the molecule to induce reaction. In this section, we discuss the electromagnetic effect enhancing the semiconductor efficiency for charge-carrier generation.

The oscillating dipole induced on a plasmonic nanoparticle under illumination produces radiation that significantly modifies the electromagnetic field associated with incoming photons under the resonance condition.[41] For instance, the intensity of the electric field is about 10^2-10^3 higher than the incoming photon flux at the surface of an isolated Ag nanoparticle (75 nm) and 10^4–10^5 between two Ag nanoparticles separated by a distance of 1 nm (**Fig. 2a**).[28] This enhanced oscillating electromagnetic field, localized close to the surface of a nanoparticle is referred to as *near-field*, and the region of high intensity is termed as a *hot spot*.[42] The electromagnetic field around a particle is spatially non-homogeneous *i.e.* more intense near a metal surface and decreases exponentially with distance.[43] At larger distances, the electric field is weaker, though it can scatter energy to the far-field. In metallic films, light can be converted into surface plasmon polaritons (SPP) and can be used to guide light into a nearby medium. In photocatalysis, plasmonics enhances the efficiency of charge-carrier generation in semiconductors *electromagnetically* through near-field coupling, scattering, and guided modes and are explained below.

2.1. Near-field coupling

When a semiconductor is placed close to a metal nanoparticle, it encounters the intense field near the surface (whereby the effective absorption cross-section of the semiconductor increases) and generates a large number of electron-hole pairs in semiconductor regions close to the surface.[44,45] This is a result of the energy overlap between the near-field and the bandgap of the semiconductor (**Fig. 2b**).[46] This mechanism has been variously named such as localized electromagnetic field enhancement (LEMF) and nearly filed coupling or PIRET.[40] It involves dipolar coupling between the metal and the semiconductor.[47] The rate of electron-hole pair generation in the semiconductor is proportional to the local intensity of the electric field (e^-, $h^+ \propto |E|^2$), which is enhanced by the plasmon resonance.[48,49] In the absence of plasmonic metal, electron-hole pairs generated in the bulk of the semiconductor recombine fast before they migrate to the surface (**Fig. 2c**). However, in the presence of the metal nanoparticle, LSPR reduces the thickness needed in the semiconductor to completely absorb the incident light and produces electron-hole pairs near the semiconductor surface (**Fig. 2d**).[50] The charge carriers are

readily separated from each other under the influence of the surface potential and have a shorter distance to reach the surface where they can perform efficient photocatalytic transformations.[28] This process has the limitation that it cannot enhance charge separation at energies smaller than the bandgap of the semiconductor.

The near-field coupling effect can be attained when the plasmonic metal and the semiconductor are in direct contact or when a spacer separates them. The latter arrangement would prevent charge-carrier transfer between metal and semiconductor and hence enable to study near-field coupling specifically. For example, the plasmonic near-field of the Au nanoparticle enhanced the charge-carrier generation in CdS, though Au and CdS were separated by a SiO_2 insulating layer (**Fig. 3a**), and this promotional effect was demonstrated for increasing the water-splitting activity of the CdS.[45] The low rates of plasmon dephasing in metal nanoparticles would enhance this process and small nanoparticles are more appropriate as they scatter less to the far-field.[38] This effect is extremely useful especially for semiconductors that have small carrier diffusion lengths.[51] It is worth noting that the absorption rate of the semiconductor has to be higher than the reciprocal of the plasmon decay time (~10–50 fs) for efficient near-field coupling.[52]

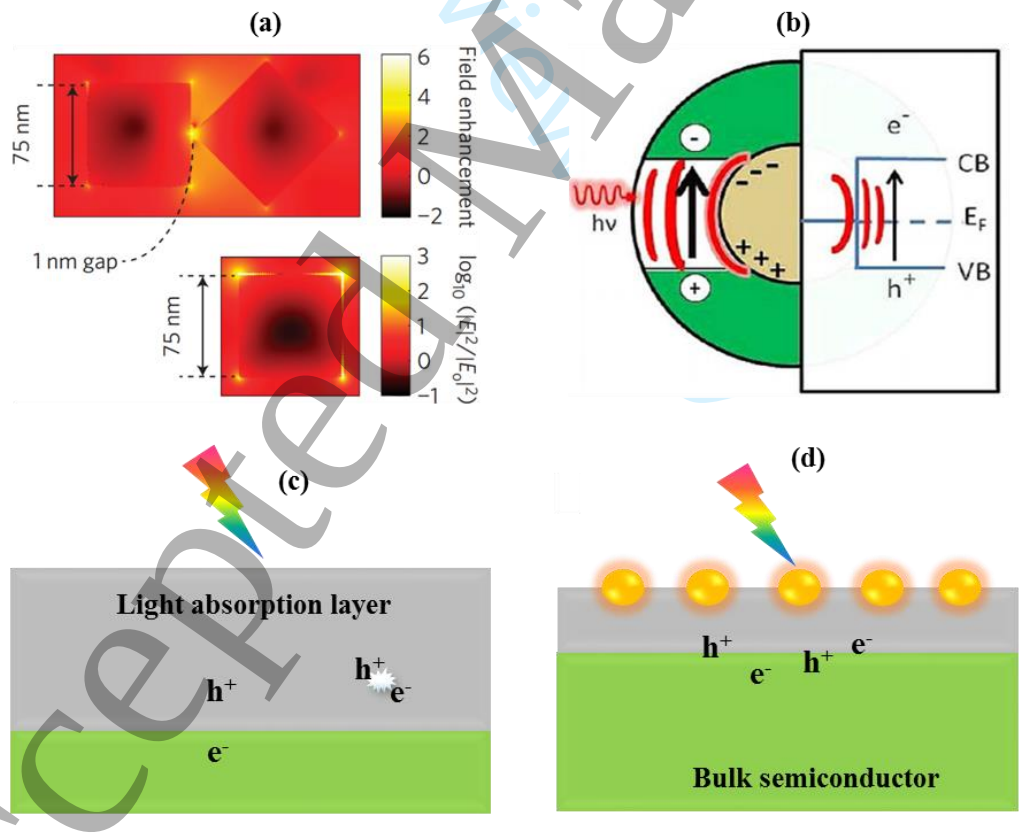

Figure 2. (a) The electric field intensity between two Ag nanocubes and an isolated Ag nanocube. Adapted with permission from ref[28]. Copyright 2011 Nature Springer. (b) Schematic representation of plasmonic near-field coupling. Adapted with permission from ref[46]. Copyright 2012 American Chemical Society. (c) Illustration of the electron-hole pair formation and recombination in the absence of plasmonic metal nanoparticles. (d) Illustration of the charge-carrier generation in the presence of

plasmonic metal nanoparticles. In this case, the light-absorption layer becomes thinner due to the near-field coupling, hence the electron-hole pairs are generated at the semiconductor surface at a high rate.

There are several reports on plasmonic near-field enhanced charge-carrier generation in semiconductors for enhancing the photocurrent generation in photovoltaic devices,[53–58] and hydrogen and oxygen production through water-splitting reaction.[59–64] Linic's group proved this effect experimentally that the intense surface plasmon resonance of Ag nanocubes (surface covered by an insulating layer) enhanced the photocatalytic H_2 evolution (**Fig. 3b**) of the nitrogen-doped TiO_2 (N-TiO_2) under visible light irradiation; in this case, the Ag LSPR spectrum (*i.e.* 400-500 nm) matched the bandgap of the N-TiO_2.[65] No such enhancement was observed when Ag was replaced by Au nanocubes as the Au LSPR does not overlap with the absorption spectrum of the N-TiO_2 (**Fig. 3c**).

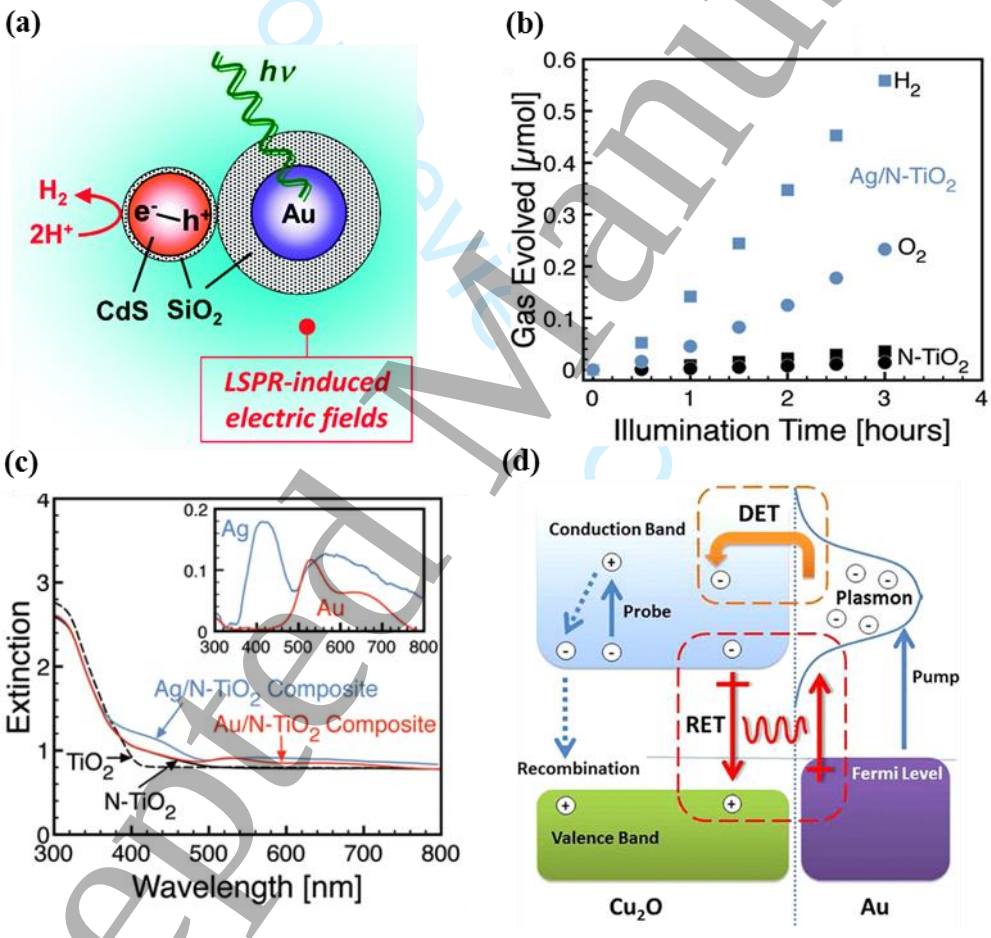

Figure 3. (a) Schematic of LSPR induced electric field in Au and the charge-carrier generation in CdS where Au and CdS are separated by an insulating layer SiO_2. Adapted with permission from ref[45]. Copyright 2011 American Chemical Society. (b) H_2 and O_2 production upon visible light illumination of N-TiO_2 (black symbols) and Ag/N-TiO_2 (blue symbols) photocatalysts, as measured by mass spectrometry. (c) UV-Vis. extinction spectra of TiO_2, N-TiO_2, Ag/N-TiO_2, and Au/N-TiO_2 samples. The inset shows different spectra for Ag and Au. Adapted with permission from ref[65]. Copyright 2011 American Chemical Society. (d) Schematic representation of the various transfer mechanisms that can occur in the Au@Cu_2O structure. Also shown in the diagram are the pump, probe (free-carrier

absorption), and recombination paths. Adapted with permission from ref[46]. Copyright 2012 American Chemical Society.

Similarly, Wu and co-workers reported the enhanced electron-hole pair generation in Cu_2O through near-field coupling by fabricating an $Au@SiO_2@Cu_2O$ sandwich system in which LSPR of Au and interband transition of Cu_2O overlapped (**Fig. 3d**).[46] To attain this effect selectively requires a spacer between plasmonic metal and semiconductor to avoid direct charge carrier transfer between metal and the semiconductor. When two metal nanoparticles are brought close to each other, coupling of their localized electromagnetic field results in the formation of hot spots where field intensity increases dramatically.[66–69] The formation and separation of electron-hole pairs in the semiconductor at such hot spots are relatively high compared to the absence of hot spots. The resonance frequency at the hot spots red-shifts with the decrease of the distance between the plasmonic nanoparticles.[70,71] This feature can guide the design of plasmonic photocatalysts with wide-range absorption. However, when the two nanoparticles are in very close contact (less than 1 nm) charge carriers can tunnel between them and the coupling will no longer be purely electromagnetic.[72] Coupling effects become much more complicated in compound plasmonic systems such as arrays and are also affected by the properties of the nearby semiconductor substrate.

2.2. Plasmonic light scattering

The charge carrier generation in the semiconductor is proportional to the local field intensity, and hence an alternate way to enhance it is by scattering more light into the semiconductor. Due to its dipolar nature, plasmonic light scattering is nearly symmetric in the forward and reverse directions when metal is embedded in a homogeneous medium.[11] However, when the metal is placed between two dielectrics (air and semiconductor) light scatters preferentially into the dielectric with the larger permittivity, which can be chosen to be the semiconductor.[73] This scattered light then acquires an angular spread in the semiconductor that effectively increases the optical path length. Moreover, the light scattered at an angle beyond the critical angle for reflection remains trapped in the semiconductor.[74] In addition, if the semiconductor has a reflecting metal back contact, light reflected towards the surface will couple to the metal nanoparticles and be partly reradiated into the semiconductor by the same scattering mechanism.[75] As a result, the incident light passes several times through the semiconductor film (**Fig. 4a**), which enhances the charge carrier generation in the semiconductor.[51] Hence, plasmonic metal is exceptionally useful to couple and trap freely propagating plane waves from the sun into an absorbing semiconductor thin film.[76] Though the underlying mechanism of

electromagnetic enhancement is similar to a near-field coupling, plasmonic light scattering can enhance carrier generation over much larger distances. Plasmonic light scattering property is commonly used in photovoltaics to produce high electric current and in catalytic water splitting to produce sustainable fuels.[65,77,78] Larger metal nanoparticles are preferred in this case, as they are dominated by scattering rather than absorption.

2.3. Guided mode through SPP

SPPs and guided modes can also be used to trap light efficiently into the semiconductor to enhance the charge carrier generation. When a corrugated metallic film is placed on the back surface of a thin semiconductor film, light is converted into SPPs which are electromagnetic waves that travel along the metal-semiconductor (**Fig. 4b**).[3,51,79] At the plasmon resonance frequency, the evanescent electromagnetic SPP fields are confined near the interface at dimensions much smaller than the wavelength.[80] SPPs excited at the metal/semiconductor interface can efficiently trap and guide light into the semiconductor layer. Moreover, the

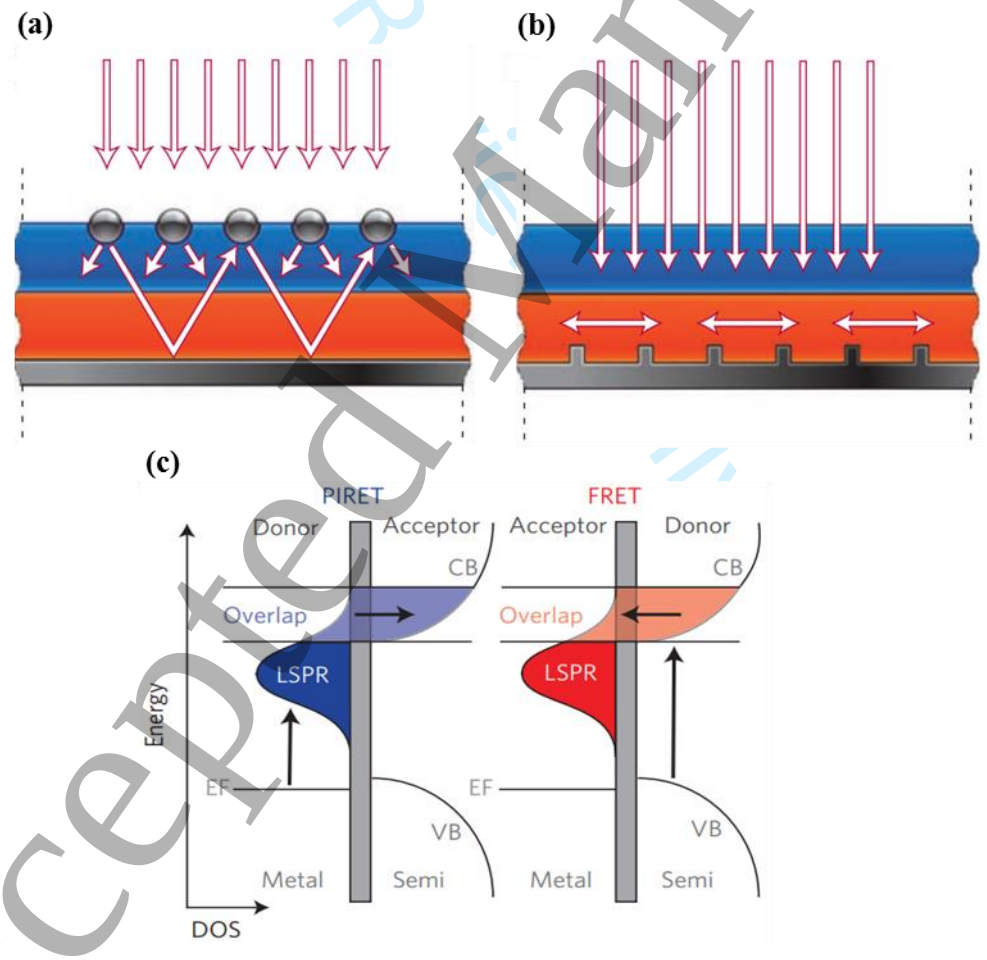

Figure 4. (a) Illustration of light scattering from metal nanoparticles, which increase the effective optical path length. (b) Schematic of surface plasmon polaritons at the metal/semiconductor interface, which propagates in the plane of the semiconductor layer. Adapted with permission from ref[81]. Copyright 2010 Nature Springer. (c) Representation of PIRET and FRET energy transfer; semiconductor is excited for

FRET and its energy transfers to the plasmonic metal. In PIRET, the plasmon is excited and its energy transfers to the semiconductor. Adapted with permission from ref[40]. Copyright 2015 Nature Springer.

incident light is effectively turned by 90° resulting in the light absorption along the lateral direction of the geometry, which has dimensions that are orders of magnitude larger than the optical absorption length.[82] This plasmonic effect is commonly used in solar cells as metal back contacts.[83–86] Guided modes can directly induce photocatalysis by guiding photons to the adsorbate that activates the reaction.

2.4. Förster resonant energy transfer (FRET)

Contrary to the electromagnetic energy transfer from a plasmonic metal to a semiconductor, incoherent energy transfer in the opposite direction from the semiconductor to the metal is also possible through dipole-dipole interaction. This process is known as fluorescence (or Förster) resonance energy transfer (FRET),[87] which is the complementary process of PIRET and can reduce the photocatalytic activity of the semiconductor. FRET is controlled by the dipole moment and dephasing time of both the semiconductor and the plasmonic metal. Wu and co-workers distinguished FRET from PIRET in a sandwich configuration, $Au@SiO_2@Cu_2O$ that the energy transfer would be symmetric if dipole moments of metal and semiconductor are equal.[40] If the semiconductor has a higher dipole moment than the metal, energy transfer from semiconductor to metal (FRET) dominates whereas PIRET would be established in the case of metal possessing a higher dipole moment (**Fig. 4c**).

3. Plasmonic hot electron-hole driven photocatalytic reactions

In addition to the above plasmonic electromagnetic effects, plasmonic metals can also directly induce photocatalysis by generating charge carriers (plasmonic hot electron-hole pairs) themselves via surface plasmon non-radiative decay. The hot electron or hole can directly enter into the adsorbate molecules or transfer into the semiconductor where a catalytic conversion occurs on the semiconductor surface.

Before discussing the mechanisms of hot electrons transfer, it is worth clarifying the term ‘hot electrons’ which is often used in different scientific fields. The name ‘hot electrons’ was originally introduced to describe non-equilibrium electrons in semiconductors whose carrier density can be described using an effective temperature term.[88,89] Electrons emitted through the photoelectric effect from the Fermi level into vacuum are also termed hot electrons.[22] The photoemitted electron simultaneously leaves a hole at its original position and both are

collectively called hot carriers as their energies are larger than those of thermal excitations at ambient temperature. They can be captured by a counter-electrode to generate electric current [90] or allowed to dissociate/desorb small molecules on the surface.[91,92] Alternatively, when an exothermic chemical reaction deposits energy on a metal surface, hot electrons can be emitted which are not in thermal equilibrium.[93] Hot electrons can also be generated in dye molecules attached to a semiconductor in dye-sensitized solar cells.[94,95]

Hot electrons in plasmonics differ from the photoelectric effect in such a way that they are distributed between Fermi and vacuum levels (**Fig. 5a**).[96] Au and Ag nanostructures were widely reported for hot-electron generation with energies between 1 eV and 4 eV under ambient conditions depending on their carrier concentration, particle size, and shape.[28,97] These hot electrons can directly enter into a nearby electron acceptor medium (semiconductor or adsorbate molecules) within femtosecond time scales.[98] In the following sub-sections, mechanisms of plasmonic hot electron-driven photocatalytic reactions are discussed in detail.

3.1. Plasmonic hot electron driven photocatalysis on the semiconductor surface

Plasmonic hot electrons can efficiently transfer into the conduction band of an appropriate semiconductor through the Schottky barrier,[99–101] which was first demonstrated by Tian and Tatsuma.[102] Tsai and co-workers reported the hot-electron transfer from a plasmonic metal to an n-type semiconductor.[103] Under dark conditions, the metal nanoparticle has a continuous Fermi–Dirac distribution of electron states, which gains energy through the non-radiative decay of LSPR under light irradiation, resulting in an electron population above the Fermi level. The electrons with energies higher than the Schottky barrier transfer into the semiconductor (**Fig. 5b**).[103] This process must occur faster than the standard Fermi-Dirac distribution re-established through electron-electron scattering.[12] In addition to the hot electron transfer through the Schottky barrier, tunnelling across the barrier can also take place, albeit with a much lower probability.[22] The energy needed for the hot electrons to overcome the Schottky barrier is considerably smaller than the bandgap of the semiconductor and hence this process permits generating charge-carriers using low-energy incident photons.[104] Once the hot electrons are transferred to the semiconductor, the metal attains a net positive charge because of electronic depletion. Electron-donor molecules can regenerate the electrons by scavenging the holes to keep the charge balance, sustaining an electric current, or running a photochemical reaction continuously.[99,105–108] This effect is highly dependent on the alignment of the band structure of the semiconductor and the Fermi level of the metal.

There were several reports on plasmonic hot electron enhanced photovoltaics[109–113] and photocatalysis,[101,114–117] often involving Au and Ag nanoparticles in contact with TiO_2.[118–122] To prove hot-electron transfer from metal to the semiconductor, Tian and Tatsuma examined the absorbance of an Au-TiO_2 film under white light illumination.[123] In an inert (N_2 saturated) medium, a gradual increase in the absorbance was observed due to the conversion of Ti^{4+} states into Ti^{3+} by hot electrons injection into TiO_2 (**Fig. 5c**).[124] When O_2 bubbled, the absorbance was decreased quickly due to the oxygen reduction by the hot electrons, which prevented the Ti^{4+} conversion. The control experiment in the absence of Au exhibited no absorbance, which further supports the claim. Furthermore, in the absence of ethanol (hole-scavenger), absorbance was higher in the beginning and reduced after 30 min (**Fig. 5d**, curves a-b) as the electrons in Au were drained over time and the transfer to TiO_2 reduced. However, as soon as ethanol was added again absorbance increased (curve c) as Au reactivated.

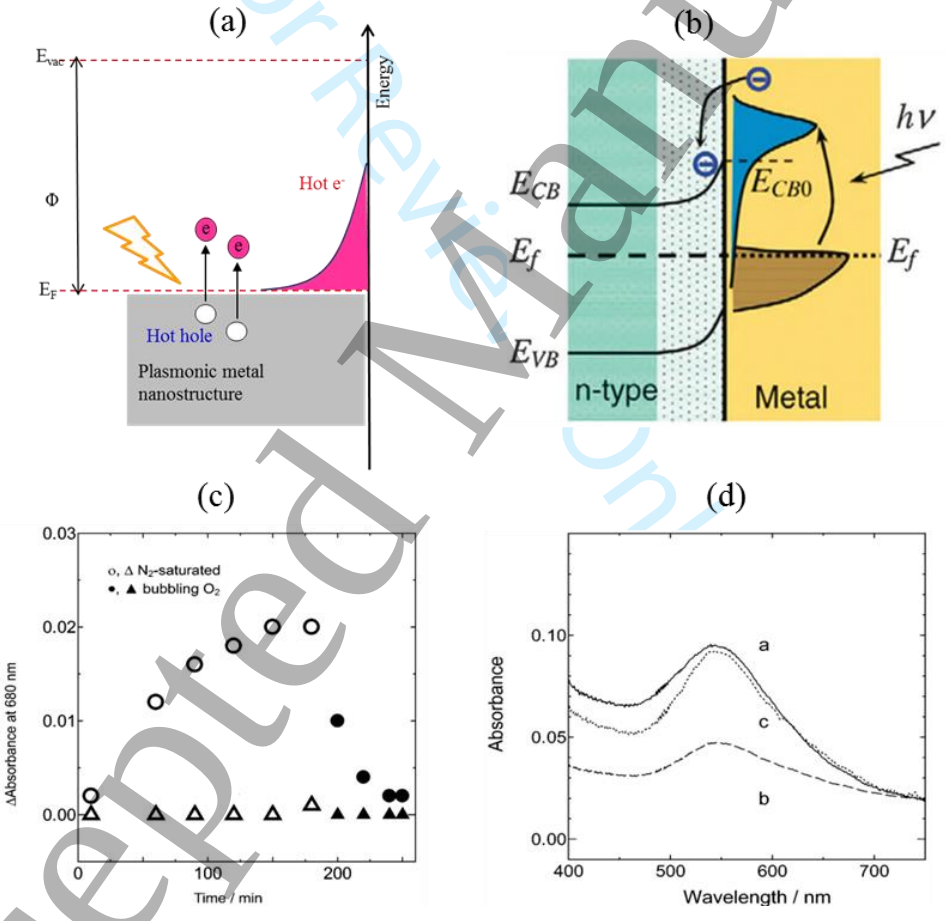

Figure 5. (a) Schematic of hot electron generation in metal nanoparticles through surface plasmon decay. (b) Light irradiation of plasmonic metal nanoparticles excites the electron from the lower energy levels to the high energy levels and then transfer them to the conduction band (CB) of the semiconductor. Adapted with permission from ref[103]. Copyright 2013 IOP Science. (c) Absorbance spectrum of the Au-TiO_2 (circles) and TiO_2 (triangles) films under white light illumination in an N_2-saturated electrolyte before and after O_2 bubbling. (d) Absorption spectra of the Au-TiO_2 in the N_2-saturated electrolyte irradiated with white light a) at the beginning, b) after 30 min, and c) ethanol added to the electrolyte. Adapted with permission from ref[123]. Copyright 2005 American Chemical Society.

It is worth noting that the plasmonic metal must be in direct contact with the semiconductor to see the hot electron-induced photocatalysis. However, near-field coupling and light scattering are inevitable in this configuration and hence one cannot say that the observed photocatalysis is only due to the hot electrons. There is however a possible way to minimize the influence of the light scattering effect by choosing small nanoparticles that have a low scattering cross-section. If the semiconductor has bandgap energy larger than the plasmonic resonance of the metal, the near-field coupling is limited. For instance, the photocatalytic reaction using 40 nm Au nanoparticles deposited over UV responsive TiO_2 under the illumination of light with a wavelength larger than 500 nm would reduce scattering and near-field coupling, such that the photocatalytic reaction observed in this case is mostly due to the hot electrons. The hot electron transfer from Au nanoparticles to the CB of the TiO_2 semiconductor followed by a photocatalytic reaction on the surface of the TiO_2 might work for dye degradation reaction, but not for H_2 generation from water splitting as TiO_2 has poor or no active sites for proton adsorption. To overcome this, a Pt cocatalyst must be deposited on the surface of TiO_2 to produce H_2.[125]

As opposed to plasmonic hot-electron transfer, the semiconductor can transfer conduction band electrons to the metal if the excitation condition activates the semiconductor rather than the metal, resulting in direct charge carrier transfer, an equivalent of FRET. A direct electron transfer from the conduction band of TiO_2 to Au nanoparticles was observed by Silva et al. under UV-light irradiation (**Fig. 6a**).[126] Linic and co-workers observed the same effect in the Ag/TiO_2 system.[28] In such cases (plasmon effects off) the metal nanoparticles are acting as cocatalysts and enhance the charge separation.

3.2. Hot-electron driven photocatalysis directly on the plasmonic metal surface

In the absence of a semiconductor, the metal nanoparticle itself can induce photocatalysis on its surface by transferring hot electrons directly into the adsorbate when the hot-electron has an energy higher than the lowest unoccupied molecular orbital (LUMO) energy of the adsorbed molecule.[127] After hot electron injection, transient ions or excited states are formed, where the adsorbate–metal system moves to a new potential energy surface and forces are induced on atoms in the adsorbate. These forces lead to the nuclear motion of atoms, which can result in the activation of chemical bonds and chemical transformations.[10] Such reactions induced by hot electrons are reduction reactions.[128] On the other hand, hot holes generated in the metal nanoparticle below the Fermi level, can induce oxidation reactions through electron transfer

from the highest occupied molecular orbital (HOMO) of the adsorbate to the holes.[129] To favour holes-driven oxidation reactions, holes must have deeper positive potential than the HOMO level of the adsorbate, otherwise, electron transfer from the molecules to the holes is prevented (**Fig. 6b**).[130] In the case of interband excitation, hot holes are generated in the d-band with energy more positive than the adsorbate HOMO levels, permitting electron transfer and inducing oxidation reactions.[131,132] In the following subsections, we discuss the hot electron-driven reduction reaction, which is driven by either indirect charge transfer (Landau damping),[133] or direct charge transfer (chemical interface damping).[134]

3.2.1. Indirect charge transfer

In the indirect charge-transfer mechanism, electron-hole pairs photogenerated on the metal surface through Landau damping with electron energies randomly distributed above the Fermi level.[135] These electrons can subsequently transfer to the adsorbate acceptor states as long as the LUMO energy matches (**Fig. 6c**). The lifetime of these high-energetic electrons is low[136–138] and they may lose energy through electron-electron scattering, resulting in a large number of low-energy electrons.[10] This suggests that indirect charge transfer is mainly due to the low-energy electrons and the photocatalytic reaction proceeds through the interactions of the adsorbate orbitals with energies close to the Fermi level of the metal. This indirect charge transfer mechanism offers limited opportunity to selectively target specific orbitals by controlling the optical properties of the nanostructure. There were several reports on hot electron-driven photocatalytic reactions on metal surfaces.[139–146] For instance, Halas and co-workers reported plasmonic Landau damping for room temperature dissociation of H_2 on Au nanoparticles embedded with TiO_2 catalyst under visible light irradiation.[147] The DFT results suggest that the hot electrons distributed above the Fermi level transfer into the antibonding orbital of the H_2 molecule. Subsequently, it creates a transient negative ion, which dissociates into atomic H by transferring the electron back to the AuNP. The same group, in the follow-up studies, used the Au-SiO_2[148] and aluminium nanocrystal[149] plasmonic configurations for H_2 dissociation reaction.

3.2.2. Direct charge transfer

In the direct charge transfer mechanism, photon absorption and charge-carrier generation are initiated by the interaction of plasmons with the accessible adsorbate electronic states.[10,135,150] As a result, hot electrons can directly enter into the higher energy LUMO orbital that matches incident photon energy, rather than first occupying available states in the metal (**Fig. 6d**). This

process is known as chemical interface damping. Linic and co-workers observed direct charge transfer in an optically excited Ag-nanocube-methylene blue (MB) system.[151] Hot electrons generated in the Ag nanoparticles are transferred directly into an unoccupied orbital with matching energy within the MB molecule (**Fig. 6e**). Surface-enhanced Raman spectroscopy (SERS) was used to distinguish the direct charge transfer effect from indirect charge transfer.

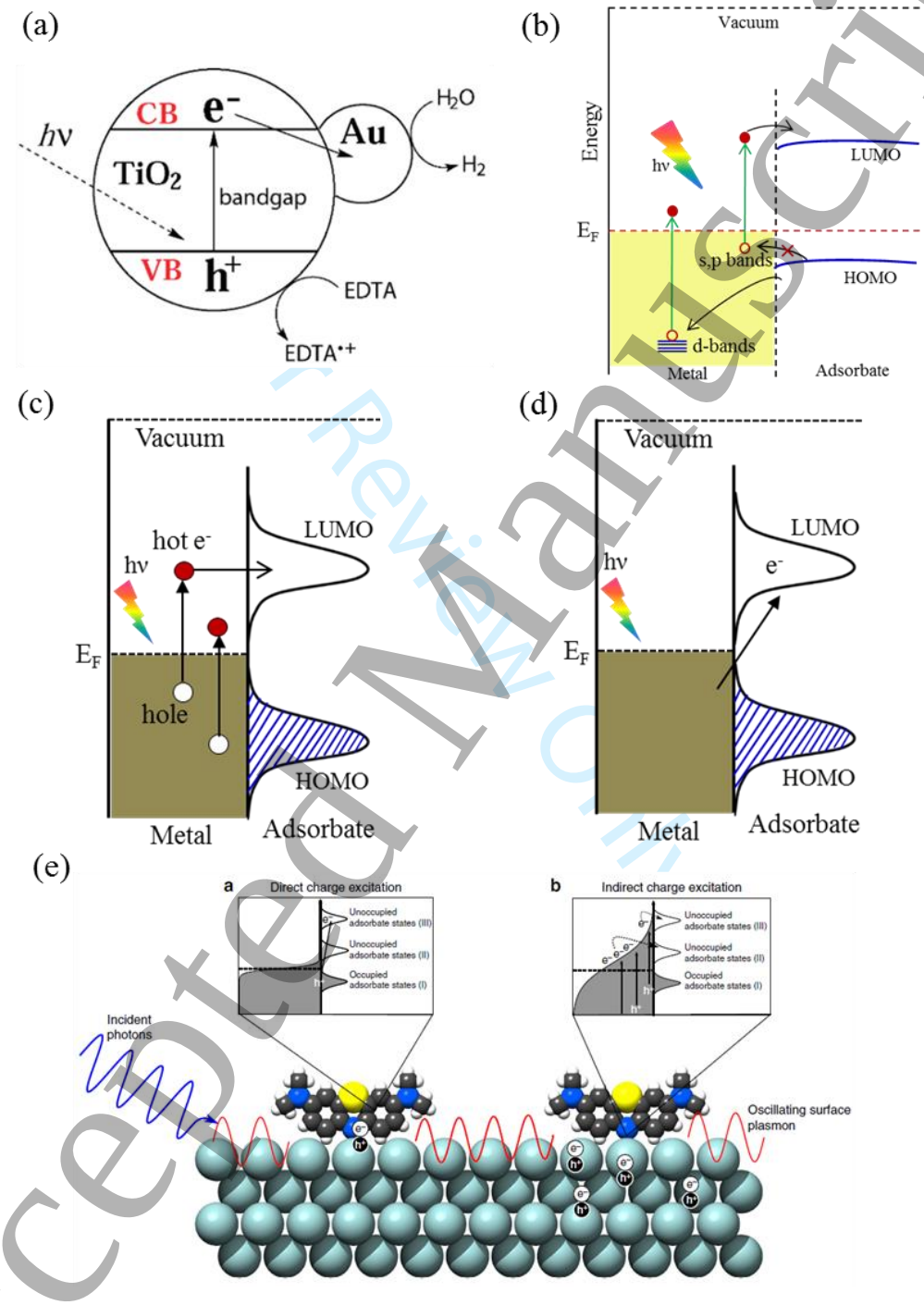

Figure 6. (a) Electron transfer from TiO_2 to Au under UV light excitation in the photocatalytic proton reduction reaction. Adapted with permission from ref[126]. Copyright 2011 American Chemical Society. (b) Illustration of the electron transfer from HOMO of the adsorbate to the hot holes resulting oxidation reaction when their energy levels are matching. (c) Schematic of indirect charge-transfer mechanism.

(d) Representation of direct charge-transfer mechanism. (e) Distinguishing direct and indirect charge transfer in Ag-MB system. Adapted with permission from ref[151]. Copyright 2016 Nature Springer.

The ratio of Anti-Stokes to Stokes scattering, which is a measure of the number of excited molecules, was found to be higher at 785 nm excitation than at 532 nm (**Fig. 7a**). If the indirect charge transfer mechanism had been dominant, the ratio would have been higher for the higher energy 532 nm irradiation. Instead, the excitation proceeds through direct charge transfer since the HOMO-LUMO energy gap reduced by chemisorption matches the photon energy at 785 nm.[152] Photocatalysis through direct charge transfer has started to receive attention due to its adsorbate orbital selectivity. However, as it is a very recent field of research, there are only limited reports discussing the subject.[153–156] Metals with resonance wavelength matching the charge excitation energy of adsorbates can accelerate chemical reactions, offering an opportunity to enhance the rate and selectivity of chemical transformations.

Though photocatalysis driven by photogenerated plasmonic hot electron transfer from metal nanoparticles to the conduction band of the semiconductor was reported,[13,157] plasmonic hot electron mediated photocatalysis directly on the metal surface is still under debate. For instance, Sivan *et al.* claimed that the earlier reports on plasmonic hot electron driven reduction reactions directly on the metal surface were purely driven by heat.[158] His group further claimed that the irradiation of metal nanoparticles may photogenerate the non-thermal electrons and holes but are less efficient to drive the chemical reaction; they demonstrated that the majority of the absorbed light heated the metal surface.[159] Indeed, it is challenging to study the temperature rise experimentally at the nanoscale. Alternatively, numerical simulation has been used, in which mostly single or few nanoparticles were assumed, although, the long-range inter-particle thermal interaction played a crucial role.[159,160] It is even more complicated during pulse radiation experiments, due to the transient nature of the temperatures and the differences between the electron and lattice temperatures.[160] On the other hand, the theoretical studies of continuous-wave irradiation mostly ignore the possibility of an increase in electron and phonon temperatures. Zhou *et al.* attempted to clarify this fact by quantifying the non-thermal carriers and thermal effects for ammonia decomposition reaction using Cu-Ru nanoparticles surrounded by a 300 μm MgO under pulsed irradiation.[161] The surface temperature of the catalyst was monitored by using a thermal imaging camera and claimed that the plasmon-mediated decomposition reaction rate was much higher than the reaction driven by the pure thermal effect. Again, this work was questioned by Sivan *et al.* that this report was not reproducible as the temperature measurement was not accurate both experimentally and numerically.[162] Based

on these discussions, we conclude that advanced pico/femtosecond spectroscopies are crucial to monitor the plasmonic hot electron transport, including from metal to the adsorbate molecules.

4. Thermo-plasmonics

Plasmonic electromagnetic effects and charge-carrier assisted photocatalysis take place at femtosecond time scales before the energetic electrons relax back to the lattice. This charge-carrier relaxation process heats the nanostructure, providing an alternative mechanism for photocatalysis. The charge carriers formed at the surface of the metal relax by interacting with electrons in the system (electron-electron scattering), resulting in an athermal charge-carrier distribution that cannot be described with a Fermi-Dirac distribution.[10] In a few hundred femtoseconds this distribution thermalizes to a Fermi-Dirac distribution with a temperature higher than the phonon temperature.[163] The thermalized electrons cool down within a few picoseconds by transferring energy to the phonon modes.[164,165] The energy transfer to the phonon modes increases the temperature of the nanoparticles which is then distributed to the environment over longer timescales.[27,166] The reaction dynamics of the photocatalysis induced by the plasmonic heating are identical to the conventional heating of nanoparticles. Even though the temperature rise through charge-carrier relaxation is small, it can induce chemical reactions.[167] There have been a few reports describing photocatalysis driven by plasmonic local heating.[168–171] For instance, Adleman and co-workers reported catalytic steam reforming of ethanol using spherical Au nanoparticles irradiated with a light of 10^7 times higher intensity than solar flux.[172] Gas bubbles were formed on the surface of the nanoparticles and the reaction taking place at the bubble-nanoparticle interface caused the reformation of ethanol. The heat produced by plasmonic nanoparticles has been widely used in the biomedical field to selectively denature various carcinomas.[173–175] For instance, Hirsch et al. treated epithelial carcinoma, a form of breast cancer, by localized heating of SiO_2–Au core-shell particles using laser light.[176]

Thermo-plasmonics is efficient in very small nanoparticles under very high intensity of light irradiation (orders of magnitude higher than solar flux) as temperature rise is proportional to the absorbed power. For larger nanoparticles, a negligible temperature increase is expected.[177] To study this effect separately from hot carriers, nanoparticles have to be irradiated using continuous-wave as it is proved to induce photocatalysis through a purely thermal effect. In the case of pulsed radiation, the reaction mechanism would follow hot-electron mediated

photocatalysis.[178] It is, however, difficult to isolate thermal effects from electromagnetic effects.

5. Chemical effect in photocatalysis

The previous sections dealt with how irradiating the plasmonic metal results in various electromagnetic, charge transfer, and thermal effects that can catalyze chemical reactions. In addition to these effects, the mere presence of the metal can have a chemical influence on the molecules and modify how they respond to any illumination. These chemical effects play an important role in photocatalysis but are often overlooked or confused with other plasmonic effects. We attempt to clarify this difference in this section.

Adsorption of the molecules on the metal surface permits breaking the molecule under low energy conditions.[152] For instance, the H_2 molecule needs 4.7 eV to dissociate in the gas phase whereas adsorption on the metal oxide surface reduces it to 2.3 eV, such that photons with 2.3 eV energy can now break the molecule.[148] The adsorbed molecule dissociates through allowable electronic transitions by absorbing photons. Plasmonic nanostructures can further enhance this process through electromagnetic effects as discussed previously. The same behaviour can also be observed in non-plasmonic metals, although these cases usually require high-energy UV photons to excite the adsorbate molecules.[179] Based on the nature of the chemical bond between adsorbate and metal, molecular dissociation from the surface can happen through intramolecular HOMO-LUMO transition and the excitation of the hybridized substrate-adsorbate bond. A weak chemical bond between the metal and the adsorbate perturbs the HOMO and LUMO energy levels of the adsorbate (**Fig. 7b**).[180] Electronic transitions can take place from HOMO to LUMO by gaining the energy from a photon matching the modified energy gap. This process of electron transfer within the adsorbate molecule is termed as intramolecular HOMO-LUMO transition. It exhibits wavelength-dependent reaction cross-sections that mimic the absorption spectra of the adsorbate molecules in the gas phase, with slightly decreased excitation energies due to metal-induced perturbations of the molecular electronic states.[181,182] There are very few reports discussing direct intramolecular HOMO−LUMO transition as the dominant mechanism in the molecular dissociation of weakly-chemisorbed adsorbates.[183,184] This kind of mechanism is less studied for plasmonic metals and represents an open research area for the future.

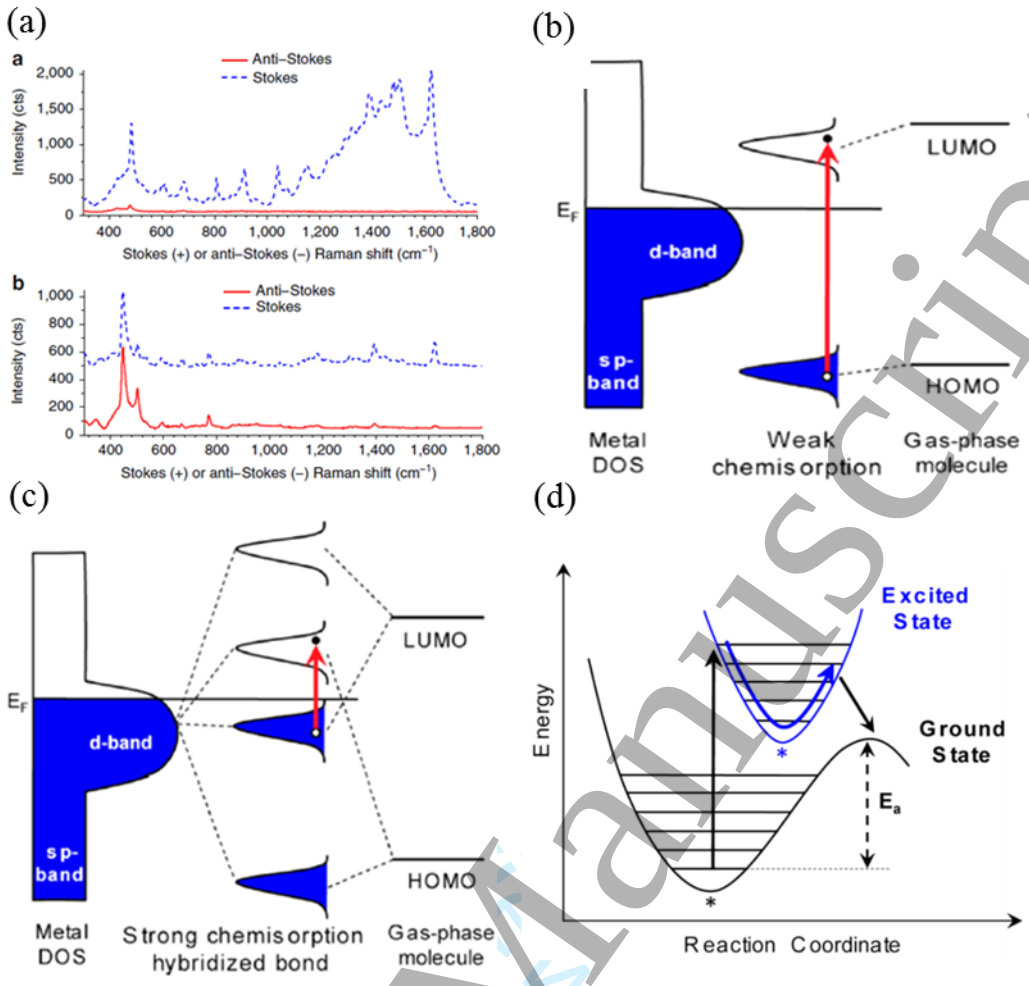

Figure 7. (a) Stokes (blue) and anti-Stokes (red) spectra for Ag nanocube–methylene blue structures observed using a 532-nm (a) or 785-nm (b) laser. Adapted with permission from ref[151]. Copyright 2016 Nature Springer. (b) Illustration of intramolecular HOMO−LUMO transitions in weakly chemisorbed systems. (c) Mechanism of direct photoexcitation of strong chemisorption bond formed between metal and adsorbate, resulting in desorption of molecules. (d) Schematic of the vibrational energy transfer into adsorbates or adsorbate−metal bonds through photo-excitation. Adapted with permission from ref[180]. Copyright 2014 American Chemical Society.

In the case of strong chemisorption between metal and adsorbate, the hybridization of metal and adsorbate orbitals forms bonding and antibonding states (**Fig. 7c**).[163,185,186] Photocatalytic dissociation of adsorbate occurs through direct electronic transitions between the hybridized bonding and antibonding states.[180] The bonding orbital has a predominant metal character while the antibonding orbital has a molecular character, such that the electron transfer is regarded as metal to the molecule.[163] Photocatalytic dissociation of water, hydrogen, oxygen, and carbon dioxide on the metal surfaces through strong chemisorption has been reported.[187–190]

Alternatively, the metal can catalyze chemical reactions involving multiple molecules by acting as a reaction site. Photocatalytic desorption of the adsorbate molecules occurs through

selectively breaking the bond between metal and adsorbate, and forming new products by combining two or more desorbed molecules.[191,192] Recently, Kale *et al.* reported CO oxidation on Pt nanoparticles in which direct photoexcitation of the Pt-CO hybridized bond was identified as the driving mechanism.[180] In the presence of O_2 and H_2, Pt forms a Pt-O bond and provides O atom through desorption that combines with desorbed CO forming CO_2. **Fig. 7d** illustrates the deposition of vibrational energy into adsorbates or adsorbate−metal bonds through photoexcitation. It promotes the system into an excited potential energy surface, where different equilibrium bond distances between the excited and ground-state potential energy surfaces induce nuclear motion, depositing vibrational energy into the system and driving reactions. Hence, the activation of targeted adsorbate−metal bonds through direct photoexcitation of hybridized electronic states enables high selectivity and opens new avenues to induce specific catalytic reactions that cannot be achieved using thermal energy.

It is worth noting that chemical effects would dominate if non-plasmonic metals are used in photocatalysis. However, in the case of photocatalysis on plasmonic metal surfaces, the overall efficiency depends on both chemical and plasmonic effects. It is possible to differentiate them by comparing the reaction rates when the molecule has direct access to the metal particle and when that direct contact is prevented using different spacers with varying chemical properties.

6. Comparison of the photoconversion efficiency of plasmonic effects

It is essential to identify which plasmonic effect is more competent to achieve high solar energy conversion (photoconversion) efficiency for photocatalysis. The interplay between the plasmonic near-field coupling, scattering, and hot electrons can be explained by plasmon dephasing including both coherent and incoherent dynamics using a density matrix model, an extended model to Shockley-Queisser limit calculations.[193] The overall photoconversion efficiency depends on the plasmon energy, the semiconductor energy and the plasmon dephasing. When the plasmon energy is higher than the bandgap energy of the semiconductor, and the plasmon dephasing time is close to the value of bulk metals (20-30 fs), the plasmonic scattering exhibits the best photoconversion. This is because the enhanced charge carrier generation in the semiconductor as scattering allows more light to be trapped in the semiconductor, which is the case for larger nanoparticles (>100 nm) as plasmons dephase radiatively upon increasing particle volume. To obtain maximum photoconversion using the scattering, the semiconductor bandgap must be close to 1.8 eV as it covers the intense portion of the solar spectrum. On the other hand, the photoconversion efficiency of hot electron transfer

into the CB of the semiconductor is high only when the semiconductor has a large bandgap (in the UV region) and the plasmon has less energy than bandgap, for instance, 1.8 eV. This effect can be realized in smaller nanoparticles (10-20 nm) with the optimal plasmon dephasing time of 3-10 fs. The photoconversion efficiency of PIRET (also known as near-field coupling or dipole-dipole coupling) is high when the plasmon energy is slightly less or near the bandgap energy of the semiconductor, and the plasmon dephasing time must be close to the dephasing time of the semiconductor. In comparison, the plasmonic near-field coupling is more efficient than hot electron injection as it can excite a few times more charge carriers in the semiconductor (**Fig. 8a**). Though plasmonic hot electron-driven photocatalysis has poor photoconversion efficiency compared to near-field coupling, the electrons transferred to the CB of the semiconductor are still hot, *i.e.* exhibit a non-thermal distribution, which has a higher thermodynamic driving force than conventional photosensitizers.[194] **Fig. 8b** shows the predicted maximum efficiency obtained for photocatalytic water splitting using the combination of all plasmonic effects compared to the semiconductor alone.

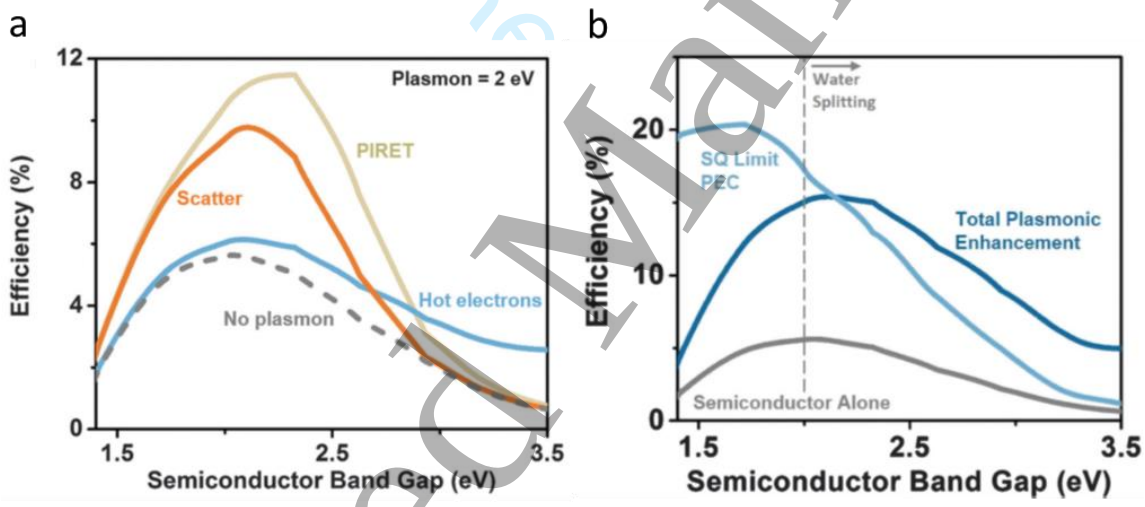

Figure 8. (a) The plasmonic enhancement mechanism responsible for the maximum conversion efficiency at a plasmon–semiconductor energy combination for photo-to-chemical conversion under AM1.5G spectrum. (b) The maximum enhancement from optimal plasmon energy and dephasing (considering the synergistic effect of all plasmonic enhancement mechanisms) compared to the semiconductor alone absorbing light and the case of 100% absorption at the band edge. The 2.0 eV bandgap required for water splitting is indicated. Adapted with permission from ref[193]. Copyright 2015 Royal Society of Chemistry.

7. Controlling the plasmonic effects

Plasmon dephasing is a crucial parameter to control the plasmonic effects for solar energy conversion including photocatalysis. For better solar energy conversion, the plasmon must have a strong dipole moment as well as cover a broad region of the solar spectrum. In contrast, the dephasing has an inverse relationship with the oscillator strength and the linewidth (**Fig. 9**). As

mentioned, the plasmon dephasing time is less than 20−30 fs and mainly depends on the nanoparticle size, shape, and material, as well as the band alignment and geometry of the metal-semiconductor heterostructures. Therefore, the balance between the near-field coupling, scattering, and hot carrier generation can be tuned by changing the materials and modifying the fabrication/morphology conditions. For instance, plasmonic scattering dominates in large nanoparticles (>100 nm) as the radiative damping increases with the volume while the dephasing time (30 fs) remains close to that of bulk metals (**Fig. 9g**).[195] When reducing the particle size to 15 nm, the near-field coupling dominates as the non-radiative damping increases in smaller particles (**Fig. 9h**); reducing the size further to 2 nm results in the dephasing of the plasmon immediately into a hot electron exhibiting a minimal optical response (**Fig. 9i**).

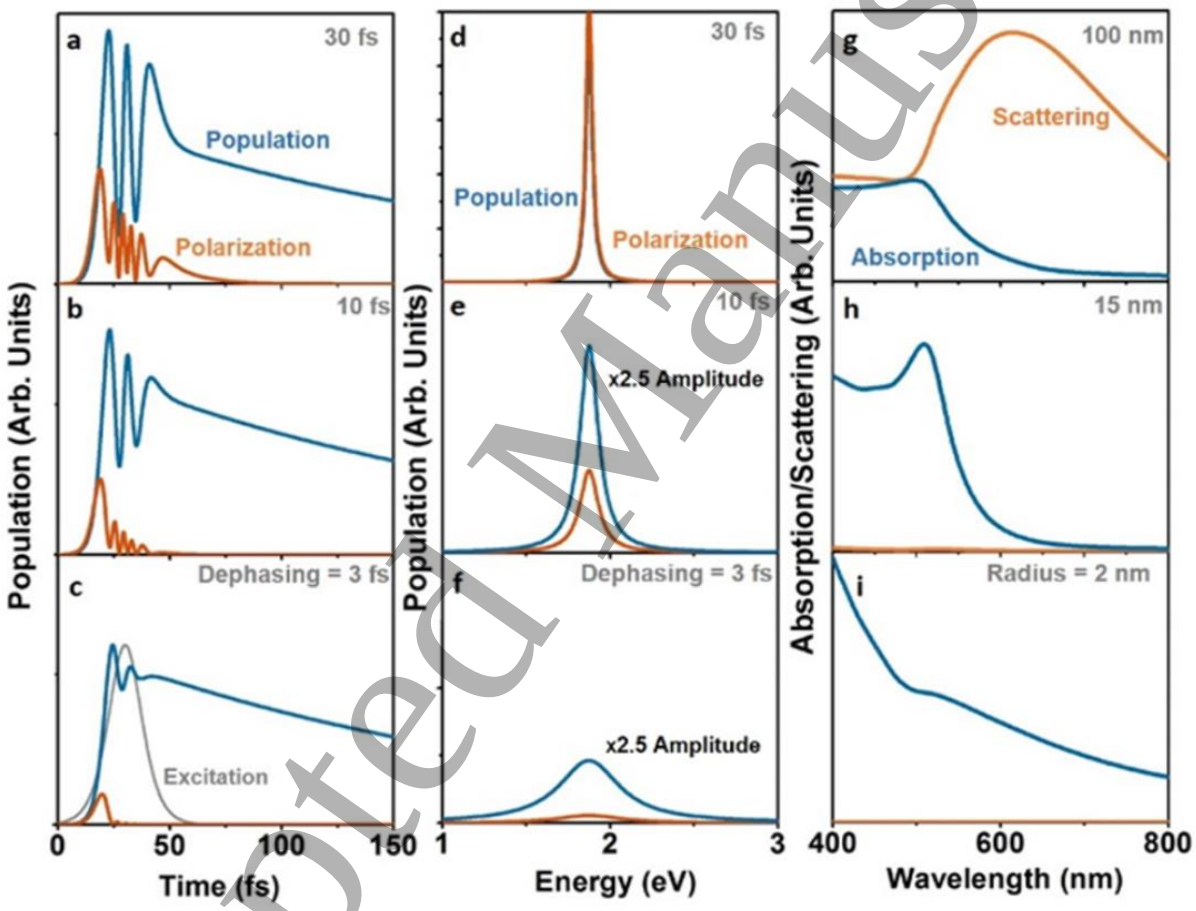

Figure 9. Effect of plasmon dephasing on optical response. (a−c) Time evolution of the plasmon and the balance between the population and polarization (related to scattering) changes with increasing dephasing rate. (d−f) Optical properties from the time evolution in part (a−c). Scattering dominates for long dephasing times; absorption dominates for short dephasing times. The peak cross-section also decreases and the line width increases with increasing dephasing rate. (g−i) The change in optical response with dephasing (parts d−f) can be related to the change in the plasmon absorption and scattering strengths with size. Small metal nanoparticles with quick dephasing times predominantly absorb incident light, whereas large metal nanoparticles with longer dephasing times predominantly scatter incident light. Adapted with permission from ref[195]. Copyright 2015 American Chemical Society.

In addition to the dephasing, fabrication conditions can also control the plasmonic effects. For instance, Cushing *et al.* have successfully demonstrated the control of plasmonic near-field coupling and hot electron injection using a time-resolved transient absorption spectroscopy (pump-probe) approach in Ag@TiO_2 and Au@TiO_2 core-shell particles (**Fig. 10**).[100] Plasmonic enhancement was determined based on the difference in the transient signal when the pump beam moved from 400 to 700 nm, recording the positive signal at each wavelength. Hot electron transfer from Au into the TiO_2 CB was selectively observed in Au@TiO_2 (**Fig. 10c**), whereas in Ag@TiO_2 structure (**Fig. 10a**) the combined effect of near-field coupling and hot electron transfer was observed due to the overlap between plasmon energy and bandgap energy of TiO_2. By depositing a ~10 nm SiO_2 dielectric layer between Ag and TiO_2, a selective near-field coupling was demonstrated in Ag@SiO_2@TiO_2 as SiO_2 prevents hot electron transfer from Ag into TiO_2 (**Fig. 10b**). In the case of depositing SiO_2 between Au and TiO_2, both hot electron injection and near-field coupling effects were absent (**Fig. 10d**).

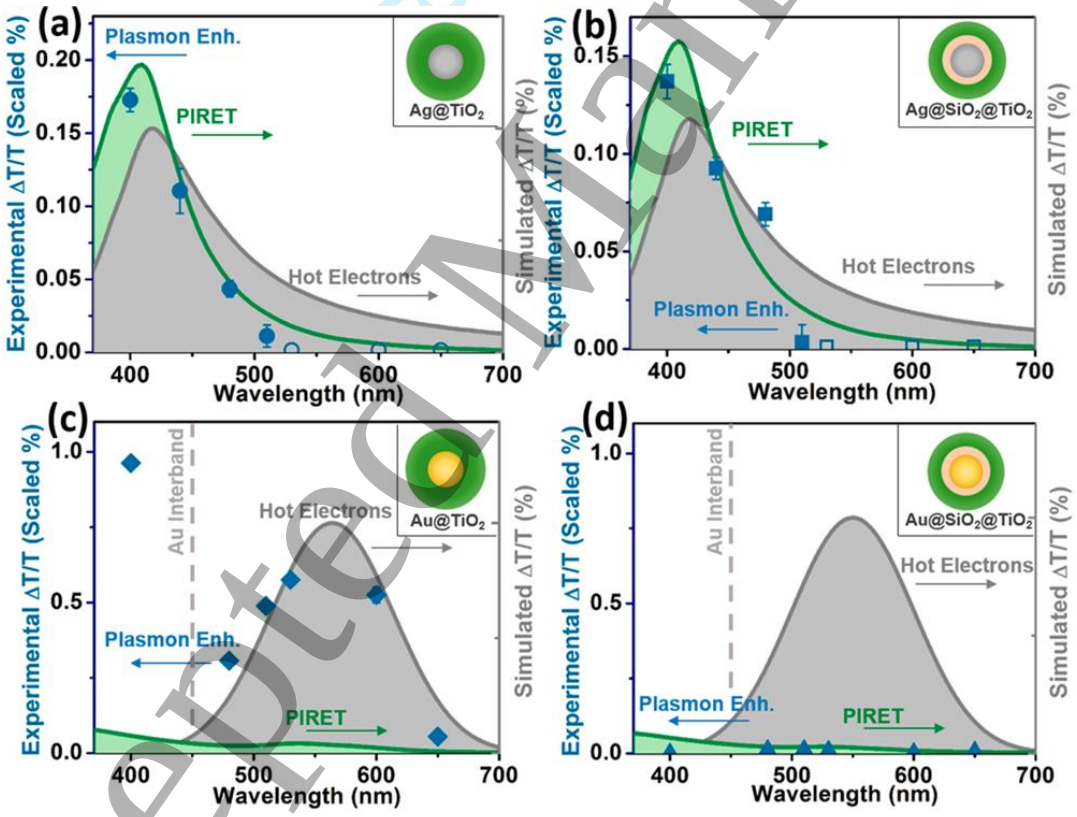

Figure 10. Control of plasmonic enhancement mechanism. The theoretical enhancement predicted for PIRET and hot electrons are shown as filled curves. (a) In Ag@TiO_2 structure, spectral overlap exists between metal and semiconductor, and PIRET and hot electron injection are measured. (b) The addition of a SiO_2 barrier to Ag@TiO_2 eliminates hot electron injection. (c) Switching the metal core to Au eliminates spectral overlap and PIRET, and hence selective hot electron enhancement. (d) Inserting a SiO_2 barrier in Au@TiO_2 eliminates both hot electron injection and PIRET despite strong light absorption by plasmonic Au. The transient absorption percentage is scaled to correct for incident power fluctuations at each wavelength. Adapted with permission from ref[100]. Copyright 2015 American Chemical Society.

8. Conclusion and outlook

In summary, we have addressed and physically distinguished the various plasmonic effects involved in photocatalysis. The incident electromagnetic field is locally amplified by the surface plasmon that can enhance photocatalysis by inducing direct optical transitions in a molecule or by improving the charge-carrier generation in the semiconductor. The electromagnetic effect influences photocatalysis through near-field coupling, plasmonic light scattering, and guided modes. Plasmonic hot carriers transferred to the semiconductor can drive photocatalysis on the surface of the semiconductor. We have attempted to clarify the confusing and often overlooked role of chemical effects in plasmonic photocatalysis. The presence of the metal particle completely changes the energy landscape in the molecule, especially in the case of hybridization of metallic and molecular orbitals. Hot carriers and chemical effects from metals, combined with their role as a reaction site and the additional electromagnetic and thermal enhancements, perform photocatalytic reactions directly on plasmonic metal surfaces and provide an exciting and promising avenue for research at the interface of physics and chemistry.

To improve the efficiency of photocatalysis, the integration of plasmonic materials with organic and inorganic semiconductors would offer more possibilities to produce economically competitive solar fuels. The optimization of the specific plasmonic effects is essential for harvesting solar energy and driving photocatalysis efficiently, which necessitates an in-depth understanding of the origin of these effects. We propose the following strategies to understand the mechanism thoroughly and improve photocatalytic efficiency: i) while numerical techniques abound in both chemistry (Ab initio molecular dynamics, density functional theories) and electromagnetics communities (FDTD, modal methods, Green's function, and FEM), it remains a challenge to combine these methods to study phenomena at the interface between chemistry and plasmonics. Efforts must be undertaken to converge both approaches, possibly using first-principles calculations on surface chemical reactions using quantum mechanical approaches as well as electromagnetic simulations; ii) a more systematic approach should be used to screen possible materials (including metals, semiconductors and molecules) and gather comprehensive information to quantify the different factors affecting the performance of plasmon-assisted photocatalytic reactions; iii) the complementary approaches from the different scientific communities is also necessary to model plasmonic enhancement of chemical reactions and design highly efficient photocatalysts comprised of plasmonic nanomaterials and semiconductors; iv) experimental techniques also need to improve their

resolution to study the charge-carrier generation and surface chemistry at fast (e.g. femtosecond) time scales; v) the type of adsorption (either chemisorption or physisorption) of molecules on the surface of the plasmonic metal or semiconductor must be studied as it represents one of the decisive factors to realise specific plasmonic effects in a controlled manner, for example chemisorption may support extracting the hot electrons directly from a plasmonic metal to the adsorbate molecules as metal and adsorbate pre-exchange the electron via chemisorption, and, hence, the electrons find an easier way to occupy the hybridized antibonding molecular orbitals; vi) hybrid antenna-reactors could be developed, in which a plasmonic metal acts as an antenna to harvest solar photons effectively and a noble metal electrocatalysts or another transition metal catalyst acts as a microreactor to produce selective fuels and high-value chemicals. We trust that the significant contribution from the above-mentioned numerical, physics and experimentally chemical engineering approaches will further advance this topic to achieve significant benchmark results in the near future.

ACKNOWLEDGMENT

M.T and O.J.F.M acknowledge the funding from Gebert Ruf Stiftung, Switzerland (Grant no. GRS-039/16). T.V.R and O.J.F.M. acknowledge funding from the European Research Commission (ERC-2015-AdG-695206 Nanofactory). M.T and J.T acknowledge funding from UK EPSRC (EP/S018204/2), Leverhulme Trust (RPG-2017-122), and Royal Society Leverhulme Trust Senior Research Fellowship (SRF\R1\21000153).

References

1. S. A. Maier, *Plasmonics: Fundamentals and Applications*, Springer US, (2007).

2. E. Stefan and N. Bonod, Eds., *Plasmonics From Basics to Advanced Topics*, Springer, (2012).

3. Heinz Raether, *Surface Plasmons on Smooth and Rough Surfaces and on Gratings*, Springer Berlin Heidelberg, (1988).

4. M. L. Brongersma and P. G. Kik, *Surface Plasmon Nanophotonics*, Springer Netherlands, (2007).

5. A. Trügler, *Optical Properties of Metallic Nanoparticles: Basic Principles and Simulation*, Springer International Publishing, (2016).

6. Y. Cao, J. Zhang, Y. Yang, Z. Huang, N.V. Long, and C. Fu, *Appl. Spectrosc. Rev.*, **50**, 499–525 (2015).

7. H. G. Rubahn, *Laser Applications in Surface Science and Technology*, Wiley, (1999).

8. J. P. Kottmann, O. J. F. Martin, D. R. Smith, and S. Schultz, *New J. Phys.*, **2**, 27 (2000).

9. W.S. Chang, B. Willingham, L.S. Slaughter, S. Dominguez-Medina, P. Swanglap, and S. Link, *Acc. Chem. Res.*, **45**, 1936–1945 (2012).

10. S. Linic, U. Aslam, C. Boerigter, and M. Morabito, *Nat. Mater.*, **14**, 567–576 (2015).

11. C. F. Bohren and D. R. Huffman, Eds., *Absorption and Scattering of Light by Small Particles*, Wiley-VCH Verlag GmbH, Weinheim, Germany, (1998).

12. S. Link and M. A. El-Sayed, *J. Phys. Chem. B*, **103**, 8410–8426 (1999).

13. A. Furube and S. Hashimoto, *NPG Asia Mater.*, **9**, e454–e454 (2017).

14. A. P. Sutton, *Electronic Structure of Materials*, Clarendon Press, (1993).

15. A. A. Maradudin, J. R. Sambles, and W. L. Barnes, *Modern Plasmonics*, Elsevier Science, (2014).

16. A. O. Govorov, H. Zhang, H. V. Demir, and Y. K. Gun'Ko, *Nano Today*, **9**, 85–101 (2014).

17. M. L. Brongersma, N. J. Halas, and P. Nordlander, *Nat. Nanotechnol.*, **10**, 25–34 (2015).

18. H. Tang, C.J. Chen, Z. Huang, J. Bright, G. Meng, R.S. Liu, and N. Wu, *J. Chem. Phys.*, **152**, 220901 (2020).

19. S. C. Warren and E. Thimsen, *Energy Environ. Sci.*, **5**, 5133–5146 (2012).

20. X. Wang and Z. M. Wang, *High-Efficiency Solar Cells: Physics, Materials, and Devices*, Springer International Publishing, (2013).

21. J. P. Kottmann, O. J. F. Martin, D. R. Smith, and S. Schultz, *Chem. Phys. Lett.*, **341**, 1–6 (2001).

22. M. L. Brongersma, N. J. Halas, and P. Nordlander, *Nat Nano*, **10**, 25–34 (2015).

23. J. Tang, *ChemSusChem*, **3**, 800–801 (2010).

24. C. Clavero, *Nat. Photonics*, **8**, 95–103 (2014).

25. S. Pillai and M. A. Green, *Sol. Energy Mater. Sol. Cells*, **94**, 1481–1486 (2010).

26. P. Zhang, T. Wang, and J. Gong, *Adv. Mater.*, **27**, 5328–5342 (2015).

27. G. Baffou and R. Quidant, *Laser Photon. Rev.*, **7**, 171–187 (2013).

28. S. Linic, P. Christopher, and D. B. Ingram, *Nat Mater*, **10**, 911–921 (2011).

29. X. Zhang, Y. Liu, S.-T. Lee, S. Yang, and Z. Kang, *Energy Environ. Sci.*, **7**, 1409–1419 (2014).

30. S. Mubeen, J. Lee, N. Singh, S. Krämer, G.D. Stucky, and M. Moskovits, *Nat. Nanotechnol.*, **8**, 247–251 (2013).

31. Y.C. Chen, Y.K. Hsu, R. Popescu, D. Gerthsen, Y.G. Lin, and C. Feldmann, *Nat. Commun.*, **9**, 232 (2018).

32. J. K. Kim, X. Shi, M.J. Jeong, J. Park, H.S. Han, S.H. Kim, Y. Guo, T.F. Heinz, S. Fan, C.L. Lee, J.H. Park, and X. Zheng, *Adv. Energy Mater.*, **8**, 1701765 (2018).

33. R. Solarska, K. Bienkowski, S. Zoladek, A. Majcher, T. Stefaniuk, P.J. Kulesza, and J. Augustynski, *Angew. Chemie Int. Ed.*, **53**, 14196–14200 (2014).

34. L. Collado, A. Reynal, F. Fresno, M. Barawi, C. Escudero, V. Perez-Dieste, J.M. Coronado, D.P. Serrano, J.R. Durrant, and V.A. de la Peña O' Shea, *Nat. Commun.*, **9**, 4986 (2018).

35. C. Xu, X. Zhang, M.N. Zhu, L. Zhang, P.F. Sui, R. Feng, Y. Zhang, and J.L. Luo, *Appl. Catal. B Environ.*, **298**, 120533 (2021).

36. J. Zhao, B. Liu, L. Meng, S. He, R. Yuan, Y. Hou, Z. Ding, H. Lin, Z. Zhang, X. Wang, and J. Long, *Appl. Catal. B Environ.*, **256**, 117823 (2019).

37. H. Robatjazi, H. Zhao, D.F. Swearer, N.J. Hogan, L. Zhou, A. Alabastri, M.J. McClain, P. Nordlander, and N.J. Halas, *Nat. Commun.*, **8**, 27 (2017).

38. S. K. Cushing and N. Wu, *J. Phys. Chem. Lett.*, **7**, 666–75 (2016).

39. S. L. Murov, I. Carmichael, and G. L. Hug, *Handbook of photochemistry*, CRC Press, (1993).

40. J. Li, S.K. Cushing, F. Meng, T.R. Senty, A.D. Bristow, and N. Wu, *Nat Phot.*, **9**, 601–607 (2015).

41. V. Giannini, A. I. Fernández-Domínguez, S. C. Heck, and S. A. Maier, *Chem. Rev.*, **111**, 3888–3912 (2011).

42. P. Muhlschlegel, H.J. Eisler, O. J. F. Martin, B. Hecht, and D.W. Pohl, *Science*, **308**, 1607–1609 (2005).

43. S. Kawata, *Near-Field Optics and Surface Plasmon Polaritons*, Springer, (2001).

44. W. Hou, Hou, W.H. Hung, P. Pavaskar, A. Goeppert, M. Aykol, and S.B. Cronin, *ACS Catal.*, **1**, 929–936 (2011).

45. T. Torimoto, H. Horibe, T. Kameyama, K. Okazaki, S. Ikeda, M. Matsumura, A. Ishikawa, and H. Ishihara, *J. Phys. Chem. Lett.*, **2**, 2057–2062 (2011).

46. S. K. Cushing, F. Meng, T.R. Senty, S. Suri, M. Zhi, M. Li, A.D. Bristow, and N. Wu, *J. Am. Chem. Soc.*, **134**, 15033–15041 (2012).

47. D. L. Andrews, *Chem. Phys.*, **135**, 195–201 (1989).

48. S. J. Lee, A. R. Morrill, and M. Moskovits, *J. Am. Chem. Soc.*, **128**, 2200–2201 (2006).

49. P. Anger, P. Bharadwaj, and L. Novotny, *Phys. Rev. Lett.*, **96**, 113002 (2006).

50. X.C. Ma, Y. Dai, L. Yu, and B.-B. Huang, *Light Sci. Appl.*, **5**, e16017 (2016).

51. H. A. Atwater and A. Polman, *Nat Mater*, **9**, 205–213 (2010).

52. V. Dusastre, *Materials for Sustainable Energy: A Collection of Peer-reviewed Research and Review Articles from Nature Publishing Group*, World Scientific, (2011).

53. J.Y. Chen, H.C. Wu, Y.C. Chiu, and W.C. Chen, *Adv. Energy Mater.*, **4**, 1301665--n/a (2014).

54. F.C. Chen, J.L. Wu, C.L. Lee, Y. Hong, C.H. Kuo, and M.H. Huang, *Appl. Phys. Lett.*, **95** (2009).

55. W.J. Yoon, K.Y. Jung, J. Liu, T. Duraisamy, R. Revur, F.L. Teixeira, S. Sengupta, and P.R. Berger, *Sol. Energy Mater. Sol. Cells*, **94**, 128–132 (2010).

56. T. L. Temple, G. D. K. Mahanama, H. S. Reehal, and D. M. Bagnall, *Sol. Energy Mater. Sol. Cells*, **93**, 1978–1985 (2009).

57. J. H. Lee, J. H. Park, J. S. Kim, D. Y. Lee, and K. Cho, *Org. Electron.*, **10**, 416–420 (2009).

58. D. Duche, P. Torchio, L. Escoubas, F. Monestier, J.J. Simon, F. Flory, and G. Mathian, *Sol. Energy Mater. Sol. Cells*, **93**, 1377–1382 (2009).

59. D. O. Sigle, L. Zhang, S. Ithurria, B. Dubertret, and J. J. Baumberg, *J. Phys. Chem. Lett.*, **6**, 1099–1103 (2015).

60. H. J. Kim, S.H. Lee, A.A. Upadhye, I. Ro, M.I. Tejedor-Tejedor, M.A. Anderson, W.B. Kim, and G.W. Huber, *ACS Nano*, **8**, 10756–10765 (2014).

61. W. R. Erwin, A. Coppola, H.F. Zarick, P. Arora, K.J. Miller, and R. Bardhan, *Nanoscale*, **6**, 12626–12634 (2014).

62. J. Qiu, G. Zeng, P. Pavaskar, Z. Li, and S. B. Cronin, *Phys. Chem. Chem. Phys.*, **16**, 3115–3121 (2014).

63. S. Shuang, R. Lv, Z. Xie, and Z. Zhang, *Sci. Rep.*, **6**, 26670 (2016).

64. L. Wang, X. Zhou, N. T. Nguyen, and P. Schmuki, *ChemSusChem*, **8**, 618–622 (2015).

65. D. B. Ingram and S. Linic, *J. Am. Chem. Soc.*, **133**, 5202–5205 (2011).

66. P. K. Jain and M. A. El-Sayed, *Chem. Phys. Lett.*, **487**, 153–164 (2010).

67. D. Radziuk and H. Moehwald, *Phys. Chem. Chem. Phys.*, **17**, 21072–21093 (2015).

68. C. P. Byers, H. Zhang, D.F. Swearer, M. Yorulmaz, B.S. Hoener, D. Huang, A. Hoggard, W.S. Chang, P. Mulvaney, E. Ringe, N.J. Halas, P. Nordlander, S. Link, and C.F. Landes, *Sci. Adv.*, **1** (2015).

69. M. Pelton and G. W. Bryant, *Introduction to Metal-Nanoparticle Plasmonics*, Wiley, (2013).

70. H. Fischer and O. J. F. Martin, *Opt. Express*, **16**, 9144–9154 (2008).

71. I. Thomann, B.A. Pinaud, Z. Chen, B.M. Clemens, T.F. Jaramillo, and M.L. Brongersma, *Nano Lett.*, **11**, 3440–3446 (2011).

72. J. A. Scholl, A. García-Etxarri, A. L. Koh, and J. A. Dionne, *Nano Lett.*, **13**, 564–569 (2013).

73. J. Mertz, *J. Opt. Soc. Am. B*, **17**, 1906–1913 (2000).

74. C. Burda, X. Chen, R. Narayanan, and M. A. El-Sayed, *Chem. Rev.*, **105**, 1025–1102 (2005).

75. B. S. Luk'yanchuk, M. I. Tribel'skiĭ, and V. V. Ternovskiĭ, *J. Opt. Technol.*, **73**, 371 (2006).

76. X. Fan, W. Zheng, and D. J. Singh, *Light Sci. Appl.*, **3**, e179 (2014).

77. M. K. Kumar, S. Krishnamoorthy, L.K. Tan, S.Y. Chiam, S. Tripathy, and H. Gao, *ACS Catal.*, **1**, 300–308 (2011).

78. P. Christopher, D. B. Ingram, and S. Linic, *J. Phys. Chem. C*, **114**, 9173–9177 (2010).

79. G. Lévêque and O. J. F. Martin, *J. Appl. Phys.*, **100**, 124301 (2006).

80. T. S. Luk, N. T. Fofang, J. L. Cruz-Campa, I. Frank, and S. Campione, *Opt. Express*, **22 Suppl 5**, A1372-9 (2014).

81. H. A. Atwater and A. Polman, *Nat. Mater.*, **9**, 205–213 (2010).

82. P. Spinelli, *J. Opt.*, **14**, 024002 (2012).

83. Y. P. Singh, A. Jain, and A. Kapoor, *J. Sol. Energy*, **2013** (2013).

84. A. Hor, Q. Luu, J. Fisher, T.S. Luk, M. Baroughi, P.S. May, and S. Smith, *2014 IEEE 40th Photovolt. Spec. Conf. PVSC 2014*, 2270–2272 (2014).

85. S. Pillai, K. R. Catchpole, T. Trupke, and M. A. Green, *J. Appl. Phys.*, **101**, 93105 (2007).

86. K. Nakayama, K. Tanabe, and H. A. Atwater, *Appl. Phys. Lett.*, **93**, 121904 (2008).

87. J. R. Lakowicz, *Principles of Fluorescence Spectroscopy*, Springer US, (2006).

88. W. A. Tisdale, K.J. Williams, B.A. Timp, D.J. Norris, E.S. Aydil, and X.Y. Zhu, *Science*, **328**, 1543–1547 (2010).

89. E. M. Conwell, *High Field Transport in Semiconductors*, Academic press, USA., (1967).

90. U. Bovensiepen, H. Petek, and M. Wolf, *Dynamics at Solid State Surfaces and Interfaces: Volume 1 - Current Developments*, Wiley, (2010).

91. A. R. Burns, E. B. Stechel, and D. R. Jennison, *Desorption Induced by Electronic Transitions DIET V: Proceedings of the Fifth International Workshop, Taos, NM, USA, April 1–4, 1992*, Springer Berlin Heidelberg, (2013).

92. H. L. Dai and W. Ho, *Laser Spectroscopy and Photochemistry on Metal Surfaces: (In 2 Parts)*, World Scientific, (1995).

93. Y. K. Lee, C.H. Jung, J. Park, H. Seo, G.A. Somorjai, and J.Y. Park, *Nano Lett.*, **11**, 4251–4255 (2011).

94. H. Nienhaus, *Surf. Sci. Rep.*, **45**, 1–78 (2002).

95. J. W. Gadzuk, *J. Phys. Chem. B*, **106**, 8265–8270 (2002).

96. T. V Shahbazyan and M. I. Stockman, *Plasmonics: Theory and Applications*, Springer Netherlands, (2014).

97. M. Rycenga, C.M. Cobley, J. Zeng, W. Li, C.H. Moran, Q. Zhang, D. Qin, and Y. Xia, *Chem. Rev.*, **111**, 3669–3712 (2011).

98. N. C. Brandt, E. L. Keller, and R. R. Frontiera, *J. Phys. Chem. Lett.*, **7**, 3178–3185 (2016).

99. K. Wu, W. E. Rodríguez-Córdoba, Y. Yang, and T. Lian, *Nano Lett.*, **13**, 5255–5263 (2013).

100. S. K. Cushing, J. Li, J. Bright, B.T. Yost, P. Zheng, A.D. Bristow, and N. Wu, *J. Phys. Chem. C*, **119**, 16239–16244 (2015).

101. A. Sousa-Castillo, M. Comesaña-Hermo, B. Rodríguez-González, M. Pérez-Lorenzo, Z. Wang, X.T. Kong, A.O. Govorov, and M.A. Correa-Duarte, *J. Phys. Chem. C*, **120**, 11690–11699 (2016).

102. Y. Tian and T. Tatsuma, *Chem. Commun.*, 1810–1811 (2004).

103. X. Zhang, Y. L. Chen, R.-S. Liu, and D. P. Tsai, *Rep. Prog. Phys.*, **76**, 46401 (2013).

104. M. W. Knight, H. Sobhani, P. Nordlander, and N. J. Halas, *Science (80-.).*, **332**, 702–704 (2011).

105. M. Wang, M. Ye, J. Iocozzia, C. Lin, and Z. Lin, *Adv. Sci.*, **3**, 1600024 (2016).

106. C. S. Kumarasinghe, M. Premaratne, Q. Bao, and G. P. Agrawal, *Sci. Rep.*, **5**, 12140 (2015).

107. C. Ng, J.J. Cadusch, S. Dligatch, A. Roberts, T.J. Davis, P. Mulvaney, and D.E. Gómez, *ACS Nano*, **10**, 4704–4711 (2016).

108. C. Wang and D. Astruc, *Chem. Soc. Rev.*, **43**, 7188–216 (2014).

109. F. B. Atar, E. Battal, L.E. Aygun, B. Daglar, M. Bayindir, and A.K. Okyay, *Opt. Express*, **21**, 7196–201 (2013).

110. P. Reineck, D. Brick, P. Mulvaney, and U. Bach, *J. Phys. Chem. Lett.*, 4137–4141 (2016).

111. A. Furube, L. Du, K. Hara, R. Katoh, and M. Tachiya, *J. Am. Chem. Soc.*, **129**, 14852–14853 (2007).

112. Y. Takahashi and T. Tatsuma, *Appl. Phys. Lett.*, **99**, 182110 (2011).

113. Y. Nishijima, K. Ueno, Y. Yokota, K. Murakoshi, and H. Misawa, *J. Phys. Chem. Lett.*, **1**, 2031–2036 (2010).

114. W. Fan, M. K. H. Leung, J. C. Yu, and W. K. Ho, *Molecules*, **21**, 180 (2016).

115. J. Y. Park, S. M. Kim, H. Lee, and B. Naik, *Catal. Letters*, **144**, 1996–2004 (2014).

116. J. Schneider, D. Bahnemann, J. Ye, G. L. Puma, and D. D. Dionysiou, *Photocatalysis: Fundamentals and Perspectives*, Royal Society of Chemistry, (2016).

117. J. C. C. Quintero and Y. J. Xu, *Heterogeneous Photocatalysis: From Fundamentals to Green Applications*, Springer Berlin Heidelberg, (2015).

118. D. Gong, W.C.J. Ho, Y. Tang, Q. Tay, Y. Lai, J.G. Highfield, and Z. Chen, *J. Solid State Chem.*, **189**, 117–122 (2012).

119. T. Toyoda, S. Tsugawa, and Q. Shen, *J. Appl. Phys.*, **105**, 034314 (2009).

120. E. Kowalska, O. O. P. Mahaney, R. Abe, and B. Ohtani, *Phys. Chem. Chem. Phys.*, **12**, 2344–2355 (2010).

121. E. Kowalska, R. Abe, and B. Ohtani, *Chem. Commun.*, 241–243 (2009).

122. Y. Ide, M. Matsuoka, and M. Ogawa, *J. Am. Chem. Soc.*, **132**, 16762–16764 (2010).

123. Y. Tian and T. Tatsuma, *J. Am. Chem. Soc.*, **127**, 7632–7637 (2005).

124. J. Schneider, M. Matsuoka, M. Takeuchi, J. Zhang, Y. Horiuchi, M. Anpo, and D.W. Bahnemann, *Chem. Rev.*, **114**, 9919–9986 (2014).

125. S. Choi and Y. S. Nam, *ACS Appl. Energy Mater.*, **1**, 5169–5175 (2018).

126. C. G. Silva, R. Juarez, T. Marino, R. Molinari, and H. Garcia, *J. Am. Chem. Soc.*, **133**, 595–602 (2011).

127. C. Boerigter, U. Aslam, and S. Linic, *ACS Nano*, **10**, 6108–6115 (2016).

128. W. Xie and S. Schlücker, *Nat. Commun.*, **6**, 7570 (2015).

129. L.B. Zhao, Y.F. Huang, X.M. Liu, J.R. Anema, D.Y. Wu, B. Ren, and Z.Q. Tian, *Phys. Chem. Chem. Phys.*, **14**, 12919 (2012).

130. T. Barman, A. A. Hussain, B. Sharma, and A. R. Pal, *Sci. Rep.*, **5**, 18276 (2015).

131. C. N. Berglund and W. E. Spicer, *Phys. Rev.*, **136**, A1044–A1064 (1964).

132. T. P. White and K. R. Catchpole, *Appl. Phys. Lett.*, **101** (2012).

133. A. I. David, N. Sébastien, C.J. Dias Eduardo, E. Itai, P. Cheng, K.D Efetov, B. Lundeberg Mark, P.

Romain, O. Johann, H. Jin-Yong, K. Jing, R. Englund Dirk, R.M. Peres Nuno, and L.H. Koppens Frank, *Science*, **360**, 291–295 (2018).

134. B. Foerster, A. Joplin, K. Kaefer, S. Celiksoy, S. Link, and C. Sönnichsen, *ACS Nano*, **11**, 2886–2893 (2017).

135. M. J. Kale and P. Christopher, *Science*, **349**, 587–588 (2015).

136. A. Manjavacas, J. G. Liu, V. Kulkarni, and P. Nordlander, *ACS Nano*, **8**, 7630–7638 (2014).

137. A. O. Govorov, H. Zhang, and Y. K. Gun'ko, *J. Phys. Chem. C*, **117**, 16616–16631 (2013).

138. A. M. Brown, R. Sundararaman, P. Narang, W. A. Goddard, and H. A. Atwater, *ACS Nano*, **10**, 957–966 (2016).

139. P. Christopher, H. Xin, A. Marimuthu, and S. Linic, *Nat. Mater.*, **11**, 1044–50 (2012).

140. P. Christopher, H. Xin, and S. Linic, *Nat. Chem.*, **3**, 467–472 (2011).

141. L. Cui, P. Wang, Y. Fang, Y. Li, and M. Sun, *Sci. Rep.*, **5**, 11920 (2015).

142. M. Sun and H. Xu, *Small*, **8**, 2777–2786 (2012).

143. W. H. Hung, M. Aykol, D. Valley, W. Hou, and S. B. Cronin, *Nano Lett.*, **10**, 1314–1318 (2010).

144. L. Bin Zhao, X. X. Liu, and D. Y. Wu, *J. Phys. Chem. C*, **120**, 1570–1579 (2016).

145. L. Bin Zhao, X.X. Liu, M. Zhang, Z. Liu, D.Y. Wu, and Z.Q. Tian, *J. Phys. Chem. C*, **120**, 944–955 (2016).

146. B. Wu, J. Lee, S. Mubeen, Y.S. Jun, G.D. Stucky, and M. Moskovits, *Adv. Opt. Mater.*, **4**, 1041–1046 (2016).

147. S. Mukherjee, F. Libisch, N. Large, O. Neumann, L.V. Brown, J. Cheng, J.B. Lassiter, E.A. Carter, P. Nordlander, and N.J. Halas, *Nano Lett.*, **13**, 240–247 (2013).

148. S. Mukherjee, L. Zhou, A.M. Goodman, N. Large, C. Ayala-Orozco, Y. Zhang, P. Nordlander, and N.J. Halas, *J. Am. Chem. Soc.*, **136**, 64–67 (2014).

149. L. Zhou, C. Zhang, M.J. McClain, A. Manjavacas, C.M. Krauter, S. Tian, F. Berg, H.O. Everitt, E.A. Carter, P. Nordlander, and N.J. Halas, *Nano Lett.*, **16**, 1478–1484 (2016).

150. K. Wu, J. Chen, J. R. McBride, and T. Lian, *Science*, **349**, 632–635 (2015).

151. C. Boerigter, R. Campana, M. Morabito, and S. Linic, *Nat. Commun.*, **7**, 10545 (2016).

152. M. J. Kale, T. Avanesian, and P. Christopher, *ACS Catal.*, **4**, 116–128 (2014).

153. O. A. Douglas-Gallardo, M. Berdakin, and C. G. Sánchez, *J. Phys. Chem. C*, **120**, 24389–24399 (2016).

154. P. Zijlstra, P. M. R. Paulo, K. Yu, Q.-H. Xu, and M. Orrit, *Angew. Chemie Int. Ed.*, **51**, 8352–8355 (2012).

155. C. Hendrich, J. Bosbach, F. Stietz, F. Hubenthal, T. Vartanyan, and F. Träger, *Appl. Phys. B*, **76**, 869–875 (2003).

156. C. Bauer, J.P. Abid, D. Fermin, and H. H. Girault, *J. Chem. Phys.*, **120**, 9302–9315 (2004).

157. A. Kumar, P. Choudhary, A. Kumar, P. H. C. Camargo, and V. Krishnan, *Small*, 2101638 (2021).

158. Y. Sivan, I. W. Un, and Y. Dubi, *Faraday Discuss.*, **214**, 215–233 (2019).

159. Y. Dubi and Y. Sivan, *Light Sci. Appl.*, **8**, 89 (2019).

160. Y. Dubi, I. W. Un, and Y. Sivan, *Chem. Sci.*, **11**, 5017–5027 (2020).

161. Z. Linan, F.D. Swearer, Z. Chao, R. Hossein, Z. Hangqi, H. Luke, D. Liangliang, C. Phillip, E.A. Carter, N. Peter, and N.J. Halas, *Science*, **362**, 69–72 (2018).

162. S. Yonatan, B. Joshua, U. I. Wai, and D. Yonatan, *Science (80-.).*, **364**, eaaw9367 (2019).

163. C. Frischkorn and M. Wolf, *Chem. Rev.*, **106**, 4207–4233 (2006).

164. R. H. M. Groeneveld, R. Sprik, and A. Lagendijk, *Phys. Rev. B*, **51**, 11433 (1995).

165. R. H. M. Groeneveld, R. Sprik, and A. Lagendijk, *Phys. Rev. B*, **45**, 5079–5082 (1992).

166. G. Baffou and R. Quidant, *Chem. Soc. Rev.*, **43**, 3898–907 (2014).

167. H. S. Fogler, *Essentials of Chemical Reaction Engineering*, Pearson Education, (2010).

168. G. Baffou, J. Polleux, H. Rigneault, and S. Monneret, *J. Phys. Chem. C*, **118**, 4890–4898 (2014).

169. L. Cao, D. N. Barsic, A. R. Guichard, and M. L. Brongersma, *Nano Lett.*, **7**, 3523–3527 (2007).

170. J. B. Herzog, M. W. Knight, and D. Natelson, *Nano Lett.*, **14**, 499–503 (2014).

171. T. Bora, D. Zoepfl, and J. Dutta, *Sci. Rep.*, **6**, 26913 (2016).

172. J. R. Adleman, D. A. Boyd, D. G. Goodwin, and D. Psaltis, *Nano Lett.*, **9**, 4417–4423 (2009).

173. C. M. Pitsillides, E. K. Joe, X. Wei, R. R. Anderson, and C. P. Lin, *Biophys. J.*, **84**, 4023–4032 (2003).

174. L. B. Carpin, L.R. Bickford, G. Agollah, T.K. Yu, R. Schiff, Y. Li, and R.A. Drezek, *Breast Cancer Res. Treat.*, **125**, 27–34 (2011).

175. I. H. El-Sayed, X. Huang, and M. A. El-Sayed, *Cancer Lett.*, **239**, 129–135 (2006).

176. L. R. Hirsch, R.J. Stafford, J.A. Bankson, S.R. Sershen, B. Rivera, R.E. Price, J.D. Hazle, N.J. Halas, and J.L. West, *Proc. Natl. Acad. Sci. U. S. A.*, **100**, 13549–54 (2003).

177. A. O. Govorov and H. H. Richardson, *Nano Today*, **2**, 30–38 (2007).

178. A. M. Goodman, N.J. Hogan, S. Gottheim, C. Li, S.E. Clare, and N.J. Halas, *ACS Nano* (2016).

179. W. Ho, *J. Phys. Chem.*, **100**, 13050–13060 (1996).

180. M. J. Kale, T. Avanesian, H. Xin, J. Yan, and P. Christopher, *Nano Lett.*, **14**, 5405–5412 (2014).

181. B. Hammer and J. K. Norskov, *Advances in Catalysis*,, vol. 45, 71–129, Academic Press (2000).

182. X.L. Zhou, X.-Y. Zhu, and J. M. White, *Surf. Sci. Rep.*, **13**, 73–220 (1991).

183. V. N. Ageev, *Prog. Surf. Sci.*, **47**, 55–203 (1994).

184. K. Watanabe, K. Sawabe, and Y. Matsumoto, *Phys. Rev. Lett.*, **76**, 1751–1754 (1996).

185. C. D. Lindstrom and X.-Y. Zhu, *Chem. Rev.*, **106**, 4281–4300 (2006).

186. H. Petek, *J. Chem. Phys.*, **137** (2012).

187. B. R. Wu and C. Cheng, *J. Phys. Condens. Matter*, **6**, 687 (1994).

188. V. Ponec, Z. Knor, and S. Černý, *Discuss. Faraday Soc.*, **41**, 149–161 (1966).

189. J.-M. Herrmann, *Catal. today*, **53**, 115–129 (1999).

190. J. R. Hahn and W. Ho, *J. Chem. Phys.*, **123**, 214702 (2005).

191. H. Petek, M. J. Weida, H. Nagano, and S. Ogawa, *Science*, **288**, 1402–1404 (2000).

192. M. Wolf, A. Hotzel, E. Knoesel, and D. Velic, *Phys. Rev. B*, **59**, 5926–5935 (1999).

193. S. K. Cushing, A. D. Bristow, and N. Wu, *Phys. Chem. Chem. Phys.*, **17**, 30013–30022 (2015).

194. S. K. Cushing, C.J. Chen, C.L. Dong, X.T. Kong, A.O. Govorov, R. Liu, and N. Wu, *ACS Nano*, **12**, 7117–7126 (2018).

195. S. K. Cushing and N. Wu, *J. Phys. Chem. Lett.*, **7**, 666–675 (2016).